

A Comprehensive Sulfur Chemistry Network with Excited S(¹D) and SO(¹Δ) for XODIAC Photochemical Model: Validation on Venus and Implications for Exo-Venus Atmospheres

PRIYANKUSH GHOSH ^{1,2} NAMRATA RANI ^{1,2,3} JEEHYUN YANG ⁴ KAREN WILLACY ⁵ P. B. RIMMER ⁶ AND
LITON MAJUMDAR ^{1,2}

¹*Exoplanets and Planetary Formation Group, School of Earth and Planetary Sciences, National Institute of Science Education and Research, Jatni 752050, Odisha, India*

²*Homi Bhabha National Institute, Training School Complex, Anushaktinagar, Mumbai 400094, India*

³*Departamento de Físico-Química, Facultad de Ciencias Químicas, Universidad de Concepción, Concepción, Chile*

⁴*Department of Astronomy and Astrophysics, The University of Chicago, Chicago, IL 60637, USA*

⁵*Jet Propulsion Laboratory, California Institute of Technology, 4800 Oak Grove Drive, Pasadena, CA 91109, USA*

⁶*Cavendish Laboratory, University of Cambridge, JJ Thomson Ave, Cambridge CB3 0HE, UK*

ABSTRACT

Sulfur chemistry is fundamental to understanding the structure, cloud formation, and atmospheric composition of Venus and Venus-like exoplanets. However, many key reactions involving ground- and excited-state sulfur species remain poorly characterized, and current photochemical models rely on networks that lack accurate kinetic data under high-temperature, high-CO₂ conditions. We compute kinetic parameters for reactions of ground-state S(³P) and excited-state S(¹D) with CO₂ under Venus-like conditions. These reactions form SO(³Σ), SO(¹Δ), and CO. The potential energy surfaces reveal intermediates, and temperature-dependent rate coefficients are obtained using a master-equation approach based on the chemically significant eigenvalue method. NASA 7-term polynomial coefficients are also derived for ground- and excited-state S and SO for consistent use in photochemical models. Incorporating these data into the one-dimensional photochemical model XODIAC shows that these reactions exert only a minor influence above 60 km in the Venus atmosphere due to competing pathways. The model agrees with observations for most sulfur-bearing species except S₃ and S₄. Introducing a 1 ppm near-surface atomic sulfur mixing ratio, representing a possible deep-atmosphere or surface source or account for missing sulfur processes, increases S₃ and S₄ by 1–2 orders of magnitude and improves agreement with measurements. For exo-Venus analogs with stratospheric isotherms and strong stellar irradiation, the new reactions significantly modify the vertical profiles of major sulfur species above 30 km and enhance S(¹D) and SO(¹Δ) more strongly than in scenarios with only isotherms or only irradiation. These results underscore the importance of accurate excited-state sulfur kinetics and the need for updated reaction networks when modeling Venus and exo-Venus atmospheres.

Keywords: Chemical kinetics (2233); Planetary atmospheres (1244); Atmospheric evolution (2301); Upper atmosphere (1748); Solar system terrestrial planets (797); Venus (1763)

1. INTRODUCTION

Sulfur is the tenth most abundant element in the universe and the fifth most abundant in our solar system (Lodders 2021). Besides H, C, N, and O, it is one of the most chemically reactive and volatile elements. Its chemical affinity for carbon and oxygen, along with its

variable oxidation states, makes it a versatile element of interest in astrophysical environments and planetary atmospheres (Titov et al. 2018; Moses et al. 1995; Irwin 1999; Moses et al. 2002). Some studies have also proposed sulfur as a proxy for metallicity in these regions (Kama et al. 2019; Turrini et al. 2021). In terrestrial planets of our solar system, such as Earth and Venus, sulfur occurs in diverse chemical forms, ranging from elemental sulfur to sulfur oxides, sulfur polyoxides, sulfuric acid, and its clusters (Malin 1997; Zhang et al.

2012; Titov et al. 2018). These sulfur-bearing species are expected to influence cloud and haze formation in planetary atmospheres. Furthermore, sulfur chemistry has been proposed as a potential trigger for Earth’s first Snowball Earth event, while sulfur isotopic ratios serve as key tracers of the Great Oxidation Event (Farquhar et al. 2000; Pavlov & Kasting 2002; Ono et al. 2003; Macdonald & Wordsworth 2017; Hodgskiss et al. 2019). Sulfur is also present on other planetary bodies in our solar system, such as Jupiter’s moon Io (Spencer et al. 2000; Moses et al. 2002) and comet 67P/C-G (Calmonte et al. 2016). In addition, the gas giants of our solar system host a wide diversity of sulfur-bearing species, including sulfur oxides, carbon disulfide, and hydrogen sulfide, which play significant roles in shaping their atmospheric compositions (Moses et al. 1995; He et al. 2020; Zahnle et al. 1995). The recent detection of photochemically produced SO₂ in the atmosphere of the gas-giant exoplanet WASP-39b (Eva-Maria Ahrer 2023; Feinstein et al. 2023; Tsai et al. 2023) and H₂S in HD 189733b (Fu et al. 2024) using JWST further highlights the importance of sulfur chemistry, not only in the gas giants of our solar system but also in exoplanetary systems.

The role of sulfur in the atmosphere of Venus is critical for understanding its atmospheric evolution and its potential as a natural laboratory for exoplanetary science (Kane et al. 2019). The Venusian atmosphere contains thick cloud layers primarily composed of sulfuric acid condensates, formed through the photochemical processing of SO₂ in the presence of a CO₂-dominated atmosphere (Dai et al. 2024; Rimmer et al. 2021). These clouds, which regulate the planetary climate, may have transformed early temperate surface conditions into the current harsh and extreme environment by following evolutionary pathways distinct from those of Earth (Dai et al. 2025). Volcanic degassing, as suggested by recent Magellan observations (Herrick & Hensley 2023), may play a key role in shaping deep atmospheric chemistry by releasing sulfur-bearing species such as H₂S and SO₂. The extreme conditions created by the runaway greenhouse effect offer a natural laboratory for studying high-temperature sulfur chemistry, with implications not only for Venus but also for Venus-like exoplanets (Kane et al. 2019). The evaporation–condensation cycle of sulfur is closely coupled with vertical mixing and can affect other reactive species through radical production (Zahnle et al. 2016; Hobbs et al. 2021; Rimmer et al. 2021). Moreover, sulfur’s ability to alter the concentrations of abundant CO₂ and other major atmospheric species may introduce variations in the interpretation of abundances in models of atmospheres that previously excluded sulfur chemistry (Veillet et al. 2024).

Due to the high reactivity of sulfur, conducting experiments under astrophysical conditions is challenging. Only a limited number of laboratory studies have incorporated sulfur (He et al. 2018, 2020; Hörst et al. 2018; DeWitt et al. 2010; Farquhar et al. 2001; Reed et al. 2020, 2022, 2024). Consequently, investigations of sulfur chemistry in planetary atmospheres rely primarily on computational approaches. Incorporating sulfur into atmospheric chemistry models has substantially advanced our understanding of planetary environments, ranging from simple chemical equilibrium models with limited molecular species (e.g., Blecic et al. 2016; Mollière, P. et al. 2017; Woitke, P. et al. 2017; Stock et al. 2018; Deka et al. 2025) to complex photochemical kinetic models that include hundreds of molecular species and detailed gas-phase chemical networks with photochemistry and two- and three-body neutral-neutral processes (Allen et al. 1981; Moses et al. 2011; Venot, O. et al. 2012; Rimmer & Helling 2016; Rimmer et al. 2021; Tsai et al. 2017; Ranjan et al. 2020; Tsai et al. 2021; Hobbs et al. 2021; Krasnopolsky 2007, 2012; Yang & Hu 2024a; Bello-Arufe et al. 2025; Hu et al. 2025; Ghosh et al. 2025). Several of these models explicitly incorporate sulfur chemistry (Krasnopolsky 2007, 2012; Ranjan et al. 2020; Tsai et al. 2021; Rimmer et al. 2021; Yang & Hu 2024a; Hu et al. 2025; Wogan et al. 2025; Ghosh et al. 2025). Typically, three major classes of sulfur reactions are included in these networks: (i) oxidation pathways involving OH radicals that produce oxides or sulfuric acid, (ii) reactions with hydrocarbons that form CS_n or OCS, and (iii) polymerization of S into S_n (He et al. 2020). These reaction networks are generally constructed using Arrhenius-type rate coefficients derived from laboratory studies or *ab initio* quantum chemical calculations.

However, current sulfur reaction networks require substantial improvement to accurately describe atmospheric sulfur chemistry. This need arises from the absence of experimentally measured or quantum chemically computed kinetic data across wide temperature ranges, as well as the omission of several key reactions and processes (Hobbs et al. 2021). For example, carbon dioxide is a primary species in both thermochemical equilibrium and photochemical models (Woitke et al. 2021; Liggins 2023; Petralia et al. 2020) and serves as the dominant carbon reservoir in the Venusian atmosphere. It is also widely used as an indicator of both primary and secondary planetary atmospheres (Swain et al. 2021). Modeling studies of gas giants suggest that sulfur can reduce CO₂ abundances by up to five orders of magnitude (Moses et al. 2016; Zahnle et al. 2016), implying a strong coupling between sulfur chemistry and the observability of CO₂. Despite the importance of this

reaction, neither experimentally measured nor *ab initio* derived rate coefficients are available. In the absence of such data, very low rate coefficients of order 10^{-20} $\text{cm}^3 \text{ molecule}^{-1} \text{ s}^{-1}$ have been adopted in a few chemical networks, including EPACRIS (Yang & Hu 2024b) and KINETICS (Willacy et al. 2022). These assumptions may lead to inaccurate predictions of sulfur-bearing species in photochemical models of planetary atmospheres.

In addition, reactions involving excited-state sulfur $\text{S}(^1\text{D})$, alongside ground-state sulfur $\text{S}(^3\text{P})$, are often neglected. Long-lived excited species can be significantly more reactive than their ground-state forms, and prior work on photoexcited CO (Yang et al. 2023) shows how photoexcitation can introduce fast, otherwise inaccessible pathways that reshape the overall chemistry under photon-rich conditions. For this reason, a recent study by Veillet et al. (2025) incorporated $\text{S}(^1\text{D})$ to explore carbon–sulfur coupling in exoplanetary atmospheres, but excited-state sulfur chemistry remains largely absent from most photochemical models. Missing species such as $\text{S}(^1\text{D})$ and $\text{SO}(^1\Delta)$, their associated thermochemistry, accurate sulfur– CO_2 reaction kinetics, and newly identified photochemical pathways capable of generating these states are crucial components that need to be incorporated into future chemical networks. Including these processes is essential for quantifying their roles in Venus, where at least half a dozen sulfur-bearing species have been detected, and for assessing their implications for potentially rocky, Venus-like exoplanets.

In this study, we address these gaps by introducing the reaction between atomic sulfur (in both its ground and excited states) and carbon dioxide using high-level quantum chemical simulations. We derive kinetic parameters for these fundamental reactions and incorporate them into the XODIAC-2025 chemical network (Ghosh et al. 2025). In addition, we expand the network by proposing new reactions involving $\text{S}(^1\text{D})$, $\text{SO}(^1\Delta)$, and ground-state SO, along with additional photochemical formation pathways for these species. We extend the thermochemical database by computing NASA 7-term polynomial coefficients for $\text{S}(^1\text{D})$ and $\text{SO}(^1\Delta)$. Using this updated XODIAC-2025 network and thermochemical database, we employ the state-of-the-art one-dimensional photochemical model XODIAC (Ghosh et al. 2025) to investigate the impact of the proposed chemistry on Venus and three exo-Venus analogs. For Venus, we compare our results with observationally constrained sulfur abundances and examine how well the extended network reproduces the measured abundances of the multiple sulfur-bearing species detected to date.

This paper is organized as follows. Section 2 describes the computational methodology used to obtain the elec-

tronic structure, kinetic, and thermochemical data for the proposed sulfur chemistry, as well as the photochemical kinetics model employed in this work (Section 3). Section 4 presents the quantum chemical results, including reaction profile analyses, temperature-dependent rate coefficients, new thermochemical parameters, and their astrophysical implications for Venus and the three exo-Venus analog atmospheres. Finally, Section 5 summarizes the main findings of this study.

2. COMPUTATIONAL METHODS FOR EXTENDING THE XODIAC CHEMICAL NETWORK AND THERMOCHEMICAL DATABASE

2.1. Electronic structure calculations

The reactant system under consideration is $[\text{S} + \text{CO}_2]$, where CO_2 is in its ground electronic state ($^1\Sigma$), and atomic sulfur is examined in both the ground state $\text{S}(^3\text{P})$ and the first excited state $\text{S}(^1\text{D})$. To investigate the reaction mechanism, preliminary transition-state (TS) searches were carried out at the B3LYP-D3(BJ)/6-311++G(2d,2p) level of theory (Becke 1993; Lee et al. 1988; Krishnan et al. 1980). The geometries of all stationary points located were further refined at the M06-2X/aug-cc-pVTZ level of theory (Zhao & Truhlar 2008). Harmonic frequency analyses were performed to obtain zero-point vibrational energies (ZPEs) and to characterize local minima (no imaginary frequencies) and transition states (one imaginary frequency). For each TS, intrinsic reaction coordinate (IRC) calculations were carried out (Fukui 1981) at the M06-2X/aug-cc-pVTZ level. Single-point electronic energies were further refined at the CCSD(T)/aug-cc-pVTZ level of theory (Raghavachari et al. 1989) using the M06-2X/aug-cc-pVTZ geometries. All electronic structure calculations were performed with GAUSSIAN 16, Revision A.03 (Frisch et al. 2016).

2.2. Kinetic calculations

The rate coefficients for all reaction pathways were computed using the Master Equation System Solver (MESS) code (Georgievskii et al. 2013) based on the potential energy surfaces calculation described in Section 2.1. MESS is based primarily on Master Equation methods (Miller & Klippenstein 2006), employing phase space theory (PST) to describe barrierless reactions and transition state theory (TST) for channels involving one or more transition states (TSs) (Bao & Truhlar 2017).

Carbon dioxide was treated as the buffer gas, and the Lennard–Jones (LJ) parameters of the reactive system were taken from the literature for the analogous CO_2/O gas-phase system (Li et al. 2012). For the barrierless

channel, the long-range interaction potential was modeled as a $-C_n/R^n$ power law, where R is the distance between the two approaching fragments (in Bohr). In this case, $n = 6$, corresponding to the isotropic dispersion interaction (Fernández-Ramos et al. 2006). To obtain the potential prefactor C_6 , a rigid scan of the interaction curve was performed by varying the distance between sulfur and the oxygen atom of CO_2 at the CCSD(T)/aug-cc-pVTZ level of theory. The resulting potential energy curve was then fitted to the $-C_6/R^6$ form, yielding $C_6 = 87.05$ a.u.

Rate coefficients were calculated at a pressure of 1 bar over the temperature range 150–2000 K using the direct diagonalization approach implemented in MESS (Georgievskii et al. 2013). These values correspond to the overall reaction pathway, rather than stepwise elementary processes. The temperature-dependent rate coefficients were then fitted to the Modified Arrhenius equation (Laidler 1996):

$$k(T) = \alpha \left(\frac{T}{300} \right)^\beta \exp \left(-\frac{\gamma}{T} \right), \quad (1)$$

where α ($\text{cm}^3 \text{ molecule}^{-1} \text{ s}^{-1}$), β , and γ (K) are the fitted parameters.

2.3. Thermochemistry calculations

A critical requirement for assessing the implications of newly computed reactions in photochemical kinetics models for planetary atmospheres is the inclusion of both forward and reverse reactions to establish equilibrium kinetics. Consequently, most photochemical kinetics models in the planetary and exoplanetary community employ NASA polynomial coefficients (Burcat & Ruscic 2005) to obtain reverse rates. For the reactions studied here, however, such coefficients describing the thermochemical parameters are not available for $\text{S}({}^1\text{D})$ and $\text{SO}({}^1\Delta)$. To compute the NASA 7-term polynomial coefficients for these species, we used *Arkane* (Automated Reaction Kinetics and Network Exploration) (Dana et al. 2023), a module of *RMG* (Gao et al. 2016; Liu et al. 2021; Johnson et al. 2022, Reaction Mechanism Generator), based on our electronic structure calculations with *GAUSSIAN 16*, Revision A.03 (Frisch et al. 2016). Because $\text{S}({}^1\text{D})$ and $\text{SO}({}^1\Delta)$ are excited states of S and SO, we performed broken-symmetry calculations in *GAUSSIAN 16* (Frisch et al. 2016) to obtain a stable single-determinant representation of the target spin state. Geometry optimizations and frequency calculations were carried out at the M06-2X/aug-cc-pVTZ level of theory. The results were then processed with *Arkane* (Dana et al. 2023), which fits NASA 7-term polynomial coefficients to thermodynamic properties, including heat

capacity, enthalpy, entropy, and Gibbs free energy, over the temperature range 10–3000 K.

3. PHOTOCHEMICAL KINETICS MODELING WITH XODIAC AND THE EXTENDED XODIAC CHEMICAL NETWORK

To assess the impact of thermochemical and photochemical sulfur kinetics on Venus and exo-Venus atmospheres, we extended the *XODIAC-2025.v1* base chemical network from Ghosh et al. (2025) by adding several new thermochemical and photochemical reactions. We refer to this expanded network as *XODIAC-2025.v2*, which incorporates both ground- and excited-state S and SO species. We simulated Venus and three exo-Venus analogs using the one-dimensional photochemistry–transport model *XODIAC* (Ghosh et al. 2025) coupled with the *XODIAC-2025.v2* network. The newly added reactions, including two-body processes and photochemical pathways, together with their relaxation channels through CO_2 and N_2 , are listed in Table 2.

For reactions 12 and 13 in Table 2, we adopted the latest JPL photochemical cross-section data (Burkholder et al. 2019), interpolating the photodissociation cross sections onto a uniform wavelength grid with 1 Å spacing over 1 to 10,000 Å. These data were supplemented with PHIDRATES cross sections (Huebner & Carpenter 1979; Huebner et al. 1992; Huebner & Mukherjee 2015). Additionally, four photochemical channels involving $\text{S}({}^1\text{D})$ and $\text{SO}({}^1\Delta)$ were included by following the analogous photochemistry of their ground states.

For the kinetic simulations, we modeled Venus and three exo-Venus scenarios using the full *XODIAC-2025.v2* thermochemical and photochemical network. For Venus, we considered four cases: (1) Model M0, which adopts the full T–P–K_{zz} profile from Krasnopolsky (2007, 2012) and employs the default *XODIAC-2025.v1* network with the lower-boundary mixing ratios from Rimmer et al. (2021). The species CO_2 , N_2 , SO_2 , H_2O , OCS , CO , HCl , H_2 , H_2S , and NO were assigned mixing ratios of 0.96, 0.03, 150 ppm, 30 ppm, 5 ppm, 20 ppm, 500 ppb, 3 ppb, 10 ppb, and 5.5 ppb, respectively. For the stellar spectrum, we used the compiled solar flux at the top of the atmosphere over 1 to 10,000 Å (Matthes et al. 2017; Coddington et al. 2015), scaled for Sun–Earth and Sun–Venus distance ratios following Rimmer et al. (2021). (2) Model M1, which is identical to M0 but includes a non-zero lower-boundary atomic sulfur abundance of 1 ppm (see Section 4.2.3). (3) Model M2, which is identical to M0 but employs the *XODIAC-2025.v2* network. (4) Model M3, which is identical to M2 but also includes a non-zero lower-boundary atomic sulfur abundance of 1 ppm (see Section 4.2.3).

For the exo-Venus analogs, we considered three scenarios: (1) Model M4, which follows the Krasnopolsky (2007) T–P profile up to approximately 30 km, with an isothermal extension at 505.6 K above this altitude, and uses the same stellar spectrum as Models M0 to M3. (2) Model M5, which is identical to M4 but receives 1000 times the solar insolation.

Table 1. Summary of all Venesian and exo-Venesian models considered in this study, including variations in the T–P profile, stellar flux, chemical network, and atomic sulfur abundance.

Model	T-P Profile	Incident Flux at TOA	Chemical Network	S mixing ratio	Model Type
M0	Krasnopolsky (2007)	1×solar	XODIAC-2025.v1	0	Venesian
M1	Krasnopolsky (2007)	1×solar	XODIAC-2025.v1	1 ppm	Venesian
M2	Krasnopolsky (2007)	1×solar	XODIAC-2025.v2	0	Venesian
M3	Krasnopolsky (2007)	1×solar	XODIAC-2025.v2	1 ppm	Venesian
M4	Krasnopolsky (2007) + 505.6 K isotherm	1×solar	XODIAC-2025.v2	0	exo-Venesian
M5	Krasnopolsky (2007)	1000×solar	XODIAC-2025.v2	0	exo-Venesian
M6	Krasnopolsky (2007) + 505.6 K isotherm	1000×solar	XODIAC-2025.v2	0	exo-Venesian

(3) Model M6, a hybrid model that uses the Krasnopolsky (2007) T–P profile with a 505.6 K isotherm above approximately 30 km together with 1000 times solar insolation. A summary of all models is provided in Table 1.

4. RESULTS

4.1. New Kinetic and Thermochemical Data and the Extended XODIAC-2025.v2 Chemical Network

4.1.1. Potential Energy Surfaces of $S(^3P) + CO_2$ and $S(^1D) + CO_2$

The potential energy surface (PES) for the studied reaction system is shown in Figure 1. We identified three pathways: Path 1 corresponds to $S(^3P) + CO_2(^1\Sigma)$, while Paths 2(a) and 2(b) correspond to $S(^1D) + CO_2(^1\Sigma)$. For Path 1, a large entrance barrier of $282.6 \text{ kJ mol}^{-1}$ is found relative to the reactants, reflecting the high stability of CO_2 in its ground state. The resulting triplet reaction complex (3RC) is an unstable thionyl formate radical [$SOCO$], formed via transition state 3TS_1 . The radical 3RC then crosses a small energy barrier of 8 kJ mol^{-1} via transition state 3TS_2 to yield the products $SO(^3\Sigma)$ and $CO(^1\Sigma)$, where $CO(^1\Sigma)$ denotes the ground state of CO . Overall, the formation of $SO(^3\Sigma)$ and $CO(^1\Sigma)$ proceeds through a two-step process, with 3RC formation being the rate-determining step in Path 1. For the remainder of this paper, the ground states of CO_2 and CO are denoted simply as CO_2 and CO .

The excitation energy required to promote ground-state sulfur $S(^3P)$ to its first excited state $S(^1D)$ is calculated to be $128.2 \text{ kJ mol}^{-1}$ at the CCSD(T)/aug-cc-pVTZ level of theory. In addition, the reacting system $S(^3P) + CO_2$ may undergo spin crossover to the singlet state $S(^1D) + CO_2$ via a minimum energy crossing point (MECP), as reported for systems involving $O(^3P)$ (Recio et al. 2022; Cavallotti et al. 2020). Since our study is limited to an adiabatic PES exploration, no attempt was made to optimize the MECP.

Furthermore, owing to the high reactivity of excited-state atomic sulfur and the identical spin multiplicities of the reactants, the formation of the singlet reaction complex in Path 2 occurs without a barrier (Figure 1). As singlet sulfur approaches carbon dioxide, its strong nucleophilic character leads to the formation of the reaction complex 1RC . Two pathways, Path 2(a) and Path 2(b), emerge from this complex, both yielding $SO(^1\Delta)$ and CO (Figure 1). In Path 2(a), 1RC dissociates via transition state $^1TS_{2a}$, which

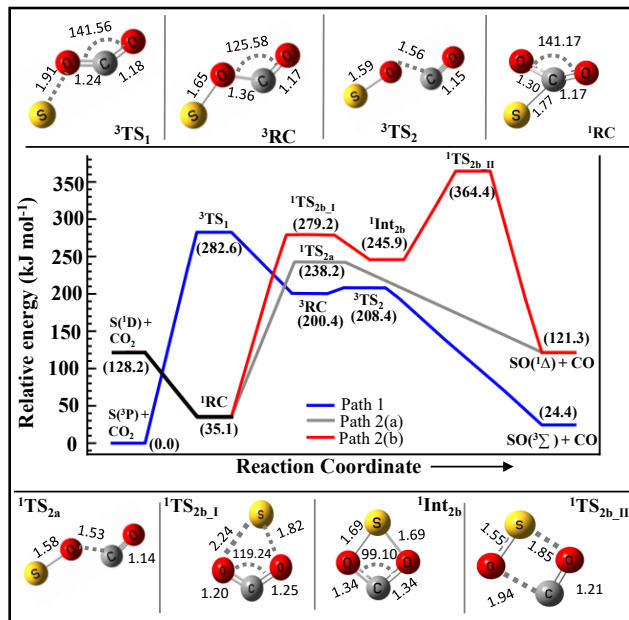


Figure 1. Reaction pathways for the $S + CO_2$ system. The relative potential energy profile (in kJ mol^{-1}) was computed at the CCSD(T)/aug-cc-pVTZ level of theory. Path 1 corresponds to the ground-state triplet surface, while Paths 2(a) and 2(b) correspond to the excited-state singlet surface. Key stationary points are labeled with their relative energies in parentheses. Optimized geometries at the M06-2X/aug-cc-pVTZ level are shown with selected bond lengths (\AA) and bond angles ($^\circ$).

has a high energy barrier of $203.1 \text{ kJ mol}^{-1}$. In Path 2(b), 1RC rearranges into a cyclic intermediate $^1Int_{2b}$ through transition state $^1TS_{2b,I}$, requiring an even higher barrier of $244.1 \text{ kJ mol}^{-1}$. This intermediate then dissociates via $^1TS_{2b,II}$, with a barrier of $118.5 \text{ kJ mol}^{-1}$, to yield the products. Both Path 2(a) and Path 2(b) are overall exothermic, although they involve very high activation barriers, partially compensated by the energy released during 1RC formation. Additional stabilization may also occur when singlet SO relaxes to its more stable triplet ground state.

4.1.2. Reaction kinetics of $S(^3P) + CO_2$ and $S(^1D) + CO_2$ and new thermochemical Data

Table 2. Newly computed and proposed two-body and photodissociation reactions added to the STAND-2020 network, incorporating S(¹D) and SO(¹Δ) chemistry. The fitted parameters are α (cm³ molecule⁻¹ s⁻¹), β , and γ (K). Numbers in parentheses denote exponents, with the values on the left representing the corresponding bases.

#	Reactions	Type	α	β	γ	Reference
1.	S + CO ₂ → SO + CO	Two-body	1.63(-13)	9.64(-1)	3.41(+4)	Path 1 in Figure 1
2.	S + CO ₂ ← SO + CO	Two-body	2.57(-20)	1.98	2.61(+4)	Path 1 in Figure 1
3.	S(¹ D) + CO ₂ → SO(¹ Δ) + CO	Two-body	4.26(-7)	-5.90(-1)	1.67(+4)	Path 2(a) in Figure 1
4.	S(¹ D) + CO ₂ ← SO(¹ Δ) + CO	Two-body	6.32(-14)	4.60(-1)	1.63(+4)	Path 2(a) in Figure 1
5.	S(¹ D) + CO ₂ → SO(¹ Δ) + CO	Two-body	2.45(-10)	9.00(-2)	3.08(+4)	Path 2(b) in Figure 1
6.	S(¹ D) + CO ₂ ← SO(¹ Δ) + CO	Two-body	5.21(-17)	1.27	2.86(+4)	Path 2(b) in Figure 1
7.	S(¹ D) + CO ₂ → S + CO ₂	Relaxation	1.00(-11)	0	0	Collision theory ¹
8.	S(¹ D) + N ₂ → S + N ₂	Relaxation	1.00(-11)	0	0	Collision theory ¹
9.	SO(¹ Δ) + CO ₂ → SO + CO ₂	Relaxation	1.00(-11)	0	0	Collision theory ¹
10.	SO(¹ Δ) + N ₂ → SO + N ₂	Relaxation	1.00(-11)	0	0	Collision theory ¹
11.	C + SO ⇌ CO + S	Two-body	1.00(-10)	0	0	KIDA ²
12.	CS ₂ + hν → CS + S(¹ D)	Photodissociation	PHIDRATES ^{3,4,5} , JPL ⁶			
13.	OCS + hν → CO + S(¹ D)	Photodissociation	PHIDRATES ^{3,4,5} , JPL ⁶			
14.	SO + hν → S(¹ D) + O	Photodissociation	PHIDRATES ^{3,4,5,7}			
15.	SO ₂ + hν → SO(¹ Δ) + O	Photodissociation	PHIDRATES ^{3,4,5,8}			
16.	S ₂ O + hν → SO(¹ Δ) + S	Photodissociation	PHIDRATES ^{3,4,5,9}			
17.	SO(¹ Δ) + hν → S + O	Photodissociation	PHIDRATES ^{3,4,5,10}			

Note.

¹ From collision theory, the pre-exponential factor for radical-radical or radical-neutral reactions assuming a barrierless potential is estimated as $\sigma(v) = \pi d^2 \times \sqrt{8k_B T / \pi m} \sim 10^{-11}$ cm³ molecule⁻¹ s⁻¹.

² Wakelam et al. (2012)

³ Huebner & Carpenter (1979), ⁴ Huebner et al. (1992), ⁵ Huebner & Mukherjee (2015), ⁶ Burkholder et al. (2019)

⁷ Assumed to be same as SO + hν → S + O

⁸ Assumed to be same as SO₂ + hν → SO + O

⁹ Assumed to be same as S₂O + hν → SO + S

¹⁰ Assumed to be same as SO + hν → S + O

Table 3. NASA 7-term polynomial coefficients for S and SO and their excited states S(¹D) and SO(¹Δ). Calculated values for S and SO molecules are shown with the the original data from Burcat & Ruscic (2005) as benchmark. First and second row correspond to the low and high temperature ranges respectively.

Species	a ₁	a ₂	a ₃	a ₄	a ₅	a ₆	a ₇
S (Burcat) (200–1000 K)	2.3173	4.7802e-03	-1.4208e-05	1.5657e-08	-5.9659e-12	3.2507e+04	6.0624
S (Burcat) (1000–6000 K)	2.8794	-5.1105e-04	2.5381e-07	-4.4546e-11	2.6672e-15	3.2501e+04	3.9814
S (this work) (10–1363.47 K)	2.5	-1.5266e-15	6.3226e-18	-7.59355e-21	2.67359e-24	32781.9	5.12978
S (this work) (1363.47–3000 K)	2.5	-1.01797e-13	8.3758e-17	-2.93808e-20	3.72101e-24	32781.9	5.12978
S(¹ D) (this work) (10–1363.47 K)	2.5	-1.5266e-15	6.3226e-18	-7.59355e-21	2.67359e-24	38222.2	4.03117
S(¹ D) (this work) (1363.47–3000 K)	2.5	-1.01797e-13	8.3758e-17	-2.93808e-20	3.72101e-24	38222.2	4.03117
SO (Burcat) (200–1000 K)	3.6186	-2.3217e-03	1.1646e-05	-1.4209e-08	5.6077e-12	-4.8062e+02	6.3650
SO (Burcat) (1000–6000 K)	3.9689	3.7730e-04	7.6710e-09	-1.3754e-11	1.3714e-15	-7.2857e+02	3.7349
SO (this work) (10–805.017 K)	3.51797	-0.00119299	8.18579e-06	-1.03275e-08	4.1527e-12	-642.697	6.72671
SO (this work) (805.017–3000 K)	3.18018	0.00226121	-1.55929e-06	4.82932e-10	-5.54866e-14	-645.852	7.9257
SO(¹ Δ) (this work) (10–835.868 K)	3.51767	-0.00113788	7.52626e-06	-9.1163e-09	3.51886e-12	6334.33	5.61013
SO(¹ Δ) (this work) (835.868–3000 K)	3.15132	0.00226302	-1.53371e-06	4.68047e-10	-5.30865e-14	6338.01	6.96758

The temperature-dependent rate coefficients for both the forward and backward directions of Path 1, S(³P) + CO₂,

and Path 2(a) and Path 2(b), S(¹D) + CO₂, are shown in

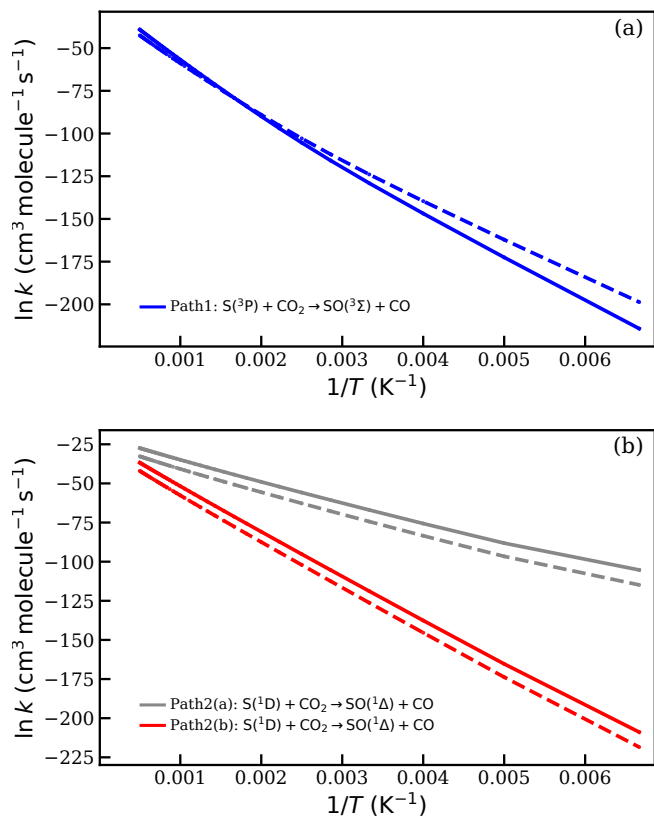


Figure 2. Calculated temperature dependence of the rate coefficients over 150 K–2000 K. — denotes the forward reaction, while - - - depicts the corresponding backward reaction.

Figure 2 for the 150–2000 K temperature range. The results clearly indicate that the formation of sulfur monoxide from $\text{S}(^3\text{P}) + \text{CO}_2$ is slower than that from the reaction of excited $\text{S}(^1\text{D})$ with CO_2 . This behavior is attributed to the high stability of carbon dioxide in its ground state, which corresponds to the large activation barrier required to form the triplet reaction complex (^3RC in Figure 1) leading to SO .

The formation of singlet sulfur monoxide proceeds faster via Path 2(a) than via Path 2(b) (Figure 1). The barrierless formation of the reaction complex (^1RC) and the smaller single-step barrier in Path 2(a) ($^1\text{TS}_{2a}$) result in higher rate coefficients compared with Path 2(b). In contrast, Path 2(b) involves two steps involving cyclization associated with substantial energy barriers, yielding rate coefficients about three orders of magnitude lower than those of Path 2(a). For both Path 2(a) and Path 2(b), the reverse reactions remain consistently slower than their forward counterparts across the entire temperature range, since the forward reaction is exothermic.

Path 1 shows an unusual trend (Figure 2). While the reverse reaction dominates at low temperatures due to its lower thermodynamic barrier, the forward rate overtakes at higher temperatures. This crossover arises from entropic contributions that reduce the activation free energy,

$$\Delta G^\ddagger = \Delta H^\ddagger - T\Delta S^\ddagger,$$

making the forward process entropically favored at low temperatures. However, it has to be noted that the rate coefficient at very low temperature ($T \leq 300$ K is highly sensitive to the uncertainty in the calculated γ term shown in Equation 1).

Table 2 summarizes the Modified Arrhenius parameters for the 150–2000 K range for the $\text{S} + \text{CO}_2$ reactant system in both ground and first excited states. While the excited-state channels may proceed through different intermediates, they all converge to the same products, $\text{SO} + \text{CO}$. Notably, the activation temperature (γ) for all pathways remain on the order of 10^4 K.

Since the photochemical kinetics model also uses Gibbs free energy to compute equilibrium constants and reverse reaction rates, we provided new thermochemical data for $\text{S}(^1\text{D})$ and $\text{SO}(^1\Delta)$. These thermodynamic parameters were first validated for the ground-state sulfur species (S and SO) using the Burcat thermochemical database, as shown in Figure 3, to assess the accuracy and reliability of our computed NASA 7-term polynomial coefficients for $\text{S}(^1\text{D})$ and $\text{SO}(^1\Delta)$, which are listed in Table 3.

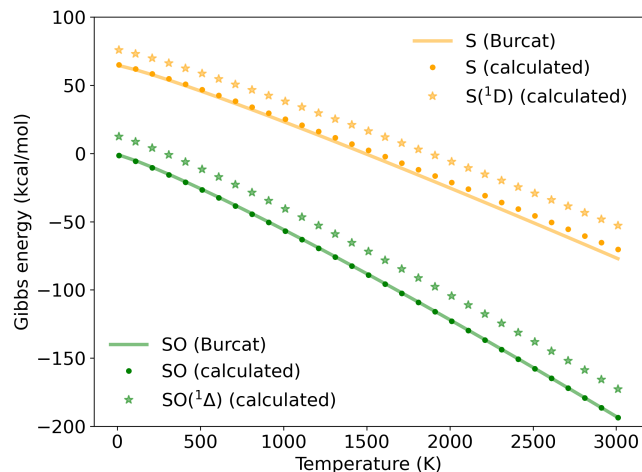


Figure 3. Comparison of Gibbs free energy (kcal/mol) as a function of temperature using NASA polynomial coefficients. Solid lines represent values from the Burcat thermochemical database (ground state), while dotted lines show ground-state values computed with Gaussian and Arkane, as listed in Table 3. The Gibbs free energies for the corresponding excited states, $\text{S}(^1\text{D})$ and $\text{SO}(^1\Delta)$, computed in this work, are shown with star-shaped markers.

4.2. Astrophysical Implications from Photochemical Kinetics Modeling with XODIAC

4.2.1. Validation of XODIAC and ARGO for Venusian Sulfur Chemistry with the XODIAC-2025 and STAND-2020 Networks

To validate our photochemical model XODIAC (Ghosh et al. 2025) for Venus using the XODIAC-2025.v1 chemical network, we benchmarked our Venusian simulations against the STAND-2020 network, which was previously used by Rimmer

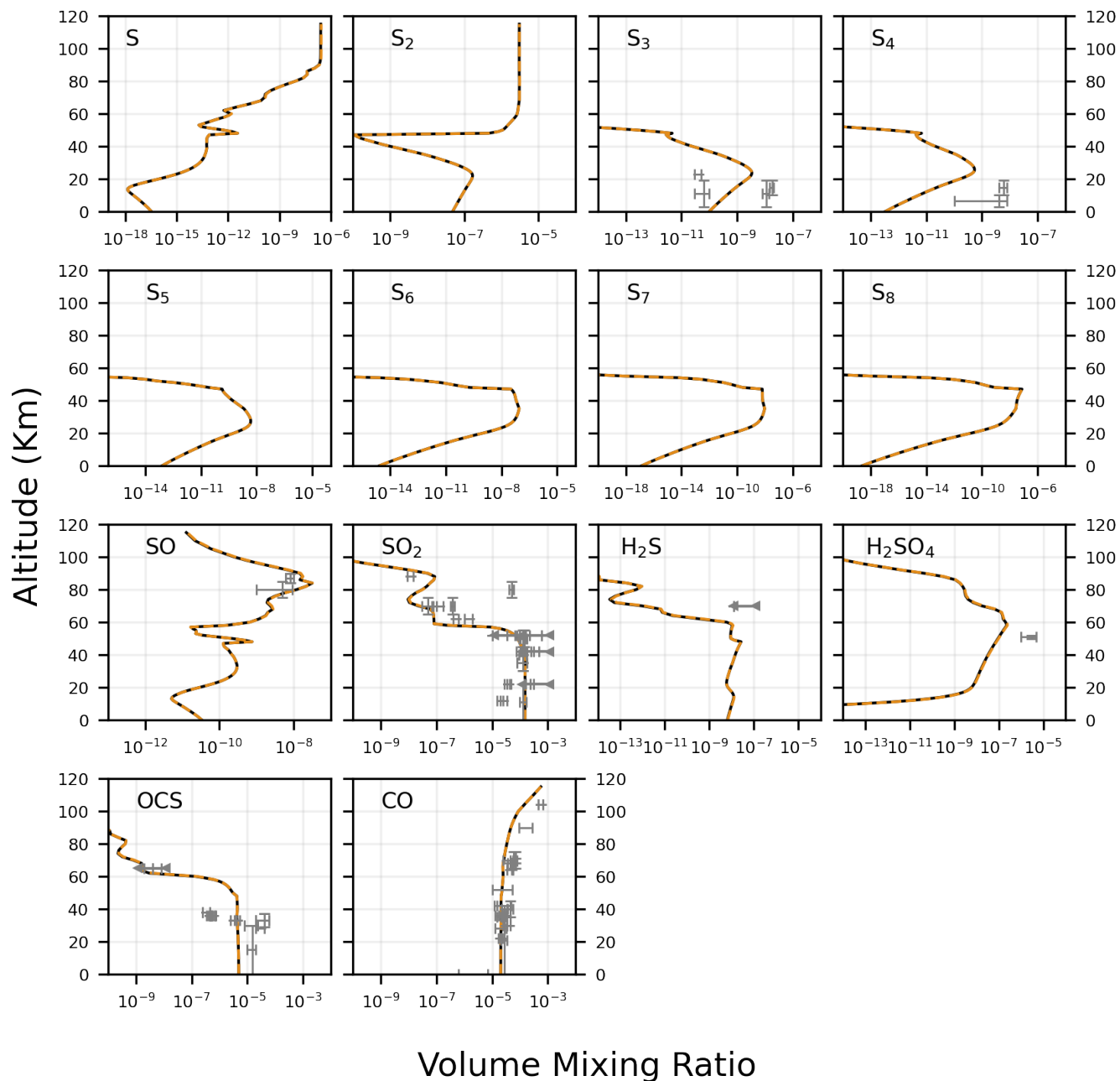


Figure 4. Predicted volume mixing ratios of S_n ($n = 1-8$), SO, SO_2 , H_2S , H_2SO_4 , OCS, and CO (including both gaseous and condensed S_2 and H_2SO_4) as a function of altitude (km) in the Venusian atmosphere, using the ARGO-STAND2020 network (solid black, similar to the cloud-chemistry model of Rimmer et al. (2021)) and the XODIAC-2025.v1 network (dashed orange). Data from various Venus missions, listed in Table 4 of Rimmer et al. (2021), are also shown in gray. Although observational data for polysulfurs S_2 , S_5 , S_6 , S_7 , and S_8 are not available, we include them to compare polysulfur chemistry between the ARGO-STAND2020 and XODIAC-2025.v1 networks, since S_3 and S_4 deviate from observed values in both cases.

et al. (2021) with the photochemical–diffusion code **ARGO**. For this comparison, we incorporated into **XODIAC** the condensation scheme based on the modified Antoine equations from Rimmer & Helling (2016); Rimmer et al. (2021), as well as the parameterization of Venus’ unknown UV absorber from Krasnopolsky (2012); Rimmer et al. (2021); Greaves et al. (2020).

For benchmarking, we adopted the same initial surface mixing ratios, T–P– K_{zz} profile, and incident solar flux at the top of the atmosphere as Rimmer et al. (2021). We find strong agreement between the **XODIAC-2025.v1** network and **ARGO+STAND-2020** for all major sulfur-bearing species in the Venusian atmosphere. The model results are shown in Figure 4, together with observed abundances from various Venus missions plotted with error bars. The observational dataset is compiled from Arney et al. (2014); Bertaux et al. (1996); Bézard et al. (1990); Bézard & de Bergh (2007); Collard et al. (1993); Connes et al. (1968); Cotton et al. (2012); Encrenaz et al. (2012, 2015); Fegley (2014); Gelman et al. (1979); Grassi et al. (2014); Greaves et al. (2020); Hoffman et al. (1980); Krasnopolsky (2008, 2010, 2013, 2014); Mairov et al. (2005); Marcq et al. (2005, 2006, 2008, 2015); Mukhin et al. (1982, 1983); Na et al. (1990); Oschlisniok et al. (2012); Oyama et al. (1979, 1980); Pollack et al. (1993); Tsang et al. (2008); Wilson et al. (1981); Young (1972); Zasova et al. (1993), as summarized by Rimmer et al. (2021).

It is evident from Figure 4 that most sulfur-bearing species are well reproduced by both **XODIAC+XODIAC-2025.v1** and **ARGO+STAND-2020**, with the exception of S_3 and S_4 .

4.2.2. Does the Extended **XODIAC** Chemical Network **XODIAC-2025.v2**, with Excited $S(^1D)$ and $SO(^1\Delta)$, Produce Observable Differences in Venusian Sulfur Chemistry?

The extended **XODIAC-2025** network **XODIAC-2025.v2** includes our calculated S–CO₂ reactions, an S–CO reaction, relaxation pathways for $S(^1D)$ and $SO(^1\Delta)$, and photochemical channels involving CS₂, OCS, SO, $SO(^1\Delta)$, SO₂, and S₂O. We now investigate whether including sulfur reaction kinetics in both ground and excited states, together with the associated reactions listed in Table 2, affects the atmospheric chemistry of Venus when modeled using **XODIAC** with the **XODIAC-2025.v2** chemical network.

We compare the modeled abundances of major sulfur-bearing species and CO using both the base **XODIAC-2025.v1** network and the extended **XODIAC-2025.v2** network, as shown in Figure 5. Observational data from various Venus missions are also plotted with error bars. It is evident from Figure 5 that most sulfur-bearing species are reproduced within observational uncertainties by the **XODIAC-2025.v2** network, similar to the base network, with the exceptions of S_3 and S_4 , which remain underproduced in both cases. This indicates that the overall Venusian sulfur chemistry remains largely unchanged even after adding the new reactions. A closer examination shows that a few photochemically active species above roughly 60 km, such as SO, SO₂, and H₂S, show small shifts in their mixing ratios, none of which alter the agreement with observed abundances. These minor variations arise primarily from differences in the rates of several

photochemical pathways. A detailed diagram of the dominant reaction pathways and their corresponding rates for SO, SO₂, and H₂S is provided in Figure 7 in the Appendix.

4.2.3. Missing Sulfur Problem on Venus

Even with the extended **XODIAC-2025.v2** network, the modeled abundances of S_3 and S_4 remain significantly lower than the observations. This discrepancy motivates a closer examination of the missing sulfur problem within both the **XODIAC-2025.v1** and **XODIAC-2025.v2** networks. In Figure 5, we therefore include cases from both networks in which a non-zero lower-boundary atomic sulfur abundance of 1 ppm is imposed. This boundary condition serves as a diagnostic of the net flux of reduced sulfur from the deep atmosphere or surface that is not explicitly represented in our model. The introduction of sulfur atoms implies that, if approximately one percent of sulfur-bearing species below the cloud layer is chemically activated and capable of releasing a sulfur atom, the observed abundances of S_3 and S_4 can be reproduced.

There are potential sources of activated sulfur that would behave similarly to the imposed atomic sulfur. One possibility is a simple mechanism in which sulfur is liberated from condensed phases into the gas phase. Perhaps atomic sulfur is being released from Venus’s surface. Less likely, the sulfur could be coming from the cloud droplets as they evaporate at the bottom of the clouds. This seems less likely because the bulk of the droplet chemistry is believed to be more oxidizing than the surrounding atmosphere (Krasnopolsky 2012; Jiang et al. 2024). The surface seems more likely, though the exchange of atoms, or really, electrons, between the lower atmosphere and the surface is uncertain: it may well be the atmosphere and surface is not in redox equilibrium (Bierson & Zhang 2020).

Another, more general possibility is that the reactive sulfur is sequestered in another chemical form. The atmosphere between 48 km and the surface may host a species capable of releasing a sulfur atom under perturbation, such as S₂O, although only if it is far more abundant than current models predict. It is also possible that, at the higher temperatures below the clouds, some sulfur chains become strained or develop terminal sulfur atoms bound by a single bond, analogous to loose threads. Although such fragments would constitute only a minor fraction of the sulfur inventory, they may nonetheless be sufficient to supply the sulfur required for this chemistry.

The S_3 and S_4 observations are highly uncertain, because it is difficult to infer specific species from such broad observed features. If the observations are accurate, then our predictions favor the presence of some lower-boundary source of active sulfur. This hypothesis can be tested either by lower-atmosphere observations of the sulfur cycle, for example, by **DAVINCI** (Garvin et al. 2022), in tandem with further laboratory and theoretical exploration into the behavior of elemental sulfur under high temperatures and thick CO₂ gas, or with minerals in contact with supercritical CO₂. In other words, exploring sulfur chemistry under simulated extreme conditions of Venus’s lower atmosphere.

Motivated by this possibility, we performed simulations using both the **XODIAC-2025.v1** and **XODIAC-2025.v2** chemical

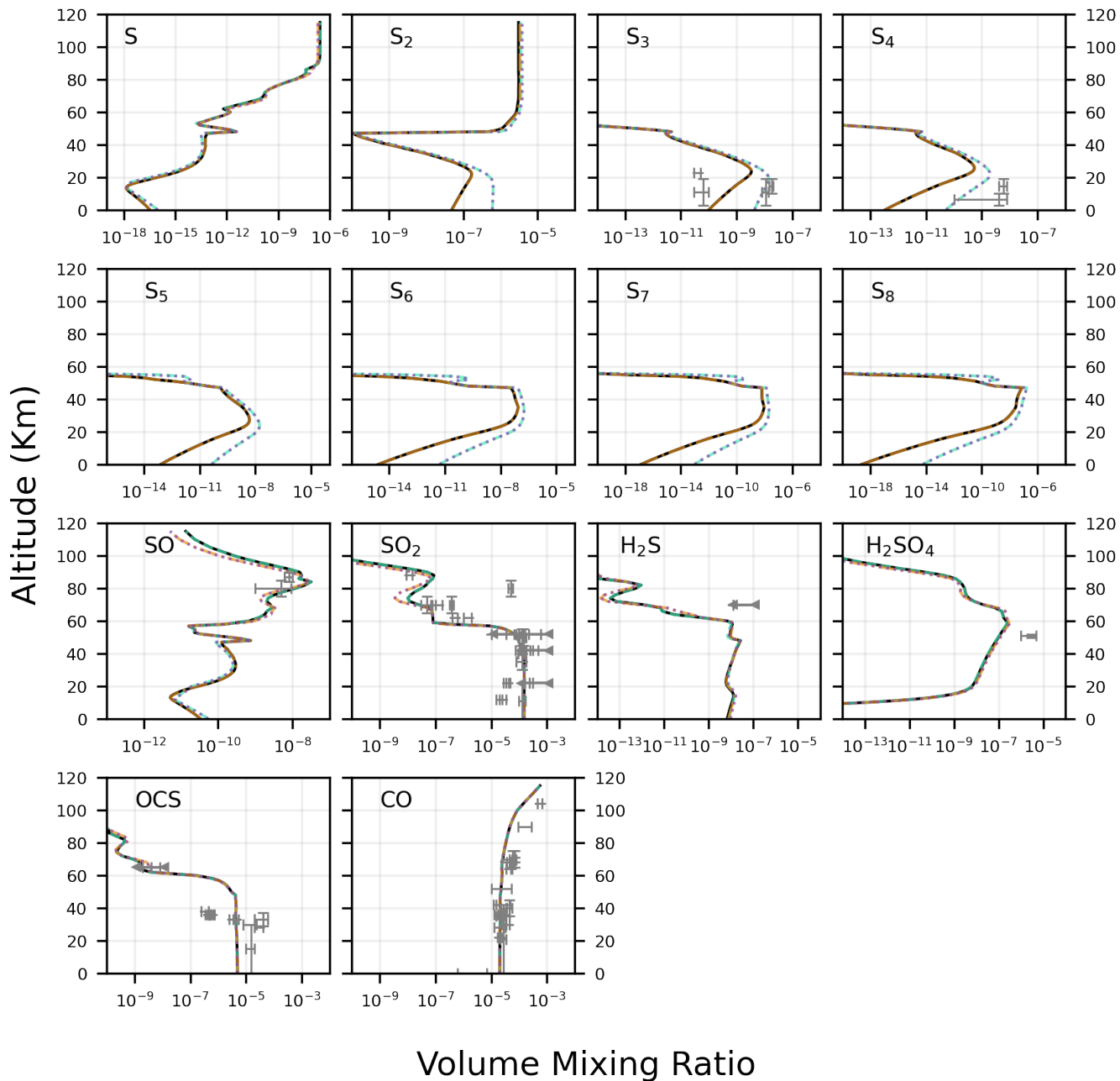


Figure 5. Predicted volume mixing ratios of S_n ($n = 1-8$), SO, SO₂, H₂S, H₂SO₄, OCS, and CO (including both gaseous and condensed S₂ and H₂SO₄) as a function of altitude (km) in the Venusian atmosphere, using the XODIAC-2025.v1 network (solid black; M0), the XODIAC-2025.v1 network with a 1 ppm surface mixing ratio of atomic sulfur (dashed green; M1), the XODIAC-2025.v2 network (dashed-dotted orange; M2), and the XODIAC-2025.v2 network with a 1 ppm surface mixing ratio of atomic sulfur (dotted purple; M3). Data from various Venus missions, listed in Table 4 of Rimmer et al. (2021), are also shown in gray. Although observational data for polysulfurs S₂, S₅, S₆, S₇, and S₈ are not available, we include them to compare polysulfur chemistry across the networks. We do not show S(¹D) and SO(¹Δ), as their mixing ratios reach a maximum of only $\sim 10^{-15}$, which lies far below observational detectability.

networks that include a non-zero lower-boundary atomic sulfur abundance. These models yield a substantially improved agreement with the observed polysulfur abundances (S_3 and S_4). In particular, the resulting near-surface mixing ratios fall within the observational error bars from Venus mission data, while producing only minor changes in the abundances of other sulfur-bearing species. We further explored initial atomic sulfur abundances in the range 10^{-8} to 10^{-5} ; however, in all such cases the resulting S_3 and S_4 vertical profiles deviated from the observational constraints, including their associated uncertainties. Notably, the abundances of polysulfurs increase by approximately a factor of two with each additional sulfur atom (S_2 , S_3 , and S_4), highlighting the non-linear nature of polysulfur chemistry driven by numerous interconversion reactions operating throughout the lower and middle atmosphere.

In regions where thermochemistry dominates, namely at pressures above 10 bar (corresponding to altitudes of approximately 30 km and below), the major reactions controlling the chemistry differ between models M0 and M1, as well as between M2 and M3. All polysulfur species (S_n) are efficiently interconverted, and the dominant reactions responsible for these processes are listed in Table 4 for S_2 , S_3 , and S_4 . At higher altitudes (around 54 km), deep within the Venusian cloud deck, condensation of sulfur species such as S_2 proceeds rapidly. The major conversion pathways operating at these altitudes are summarized in Table 5, where g and l denote gaseous and condensed (liquid) phases, respectively.

For each sulfur species, the net abundance is determined by the balance between its production and loss rates. These rates can differ by several orders of magnitude, even for the same dominant reaction across different models. For example, reaction 1 in Table 4 governs both the formation and destruction of S_2 in models M0 and M1, contributing approximately 99.8% of the total rate in both cases, yet the absolute reaction rates differ by nearly two orders of magnitude. Such discrepancies can arise even at the same altitude because the absolute rate of S_2 formation or destruction depends on the mixing ratios of all reactants involved, whereas the percentage contribution depends on the sum of all S_2 -related reaction rates within the network.

Notably, the enhanced abundance of sulfur atoms in the deep atmosphere (up to 30 km) approximately doubles the abundance of S_2 in models M1 and M3 relative to models M0 and M2, with even larger increases observed for the higher polysulfurs S_3 and S_4 .

These changes in abundance arise primarily from differences in the dominant reaction rates between models M0 and M1, and between models M2 and M3. A higher initial sulfur mixing ratio modifies the early-time production and loss rates of several species, including SO, CO, and other sulfur-bearing molecules. As the system evolves, the elevated sulfur abundance in models M1 and M3 leads to modest deviations from the corresponding abundances in models M0 and M2. These small differences propagate through the network of interconversion reactions listed in Table 4, ultimately influencing the abundances of the polysulfurs. The dominant reaction channels and their corresponding rates for S_2 , S_3 , and

Table 4. Sulfur reaction pathways at lower altitudes ($\lesssim 30$ km).

#	Reaction	Reaction Type
1.	$2S_2 + M \rightleftharpoons S_4 + M$	Three-body
2.	$S_2 + S_6 + M \rightleftharpoons S_8 + M$	Three-body
3.	$S_2 + S_3 + M \rightleftharpoons S_5 + M$	Three-body
4.	$S + S_2 + M \rightarrow S_3 + M$	Three-body
5.	$S_3 + S_6 \rightleftharpoons S_2 + S_7$	Two-body
6.	$S_3 + S_7 \rightleftharpoons S_2 + S_8$	Two-body
7.	$S_3 + S_7 \rightleftharpoons 2S_5$	Two-body
8.	$S_3 + S_7 \rightleftharpoons S_4 + S_6$	Two-body
9.	$S_4 + S_6 \rightleftharpoons S_2 + S_8$	Two-body
10.	$S_3 + S_8 \rightleftharpoons S_4 + S_7$	Two-body
11.	$S_4 \xrightarrow{h\nu} 2S_2$	Photochemical
12.	$S_4 \xrightarrow{h\nu} S_3 + S$	Photochemical

Table 5. Sulfur reaction pathways at mid-altitudes (~ 54 km).

#	Reaction	Reaction Type
1.	$S_2(g) \rightarrow S_2(l)$	Condensation
2.	$S + SNO \rightarrow S_2 + NO$	Two-body
3.	$S + OCS \rightarrow CO + S_2$	Two-body
4.	$S_3 \xrightarrow{h\nu} S_2 + S$	Photochemical
5.	$S_4 \xrightarrow{h\nu} S_3 + S$	Photochemical
6.	$S + S_8 \rightarrow S_3 + S_6$	Two-body
7.	$S + S_7 \rightarrow S_3 + S_5$	Two-body
8.	$2S_5 \rightarrow S_3 + S_7$	Two-body
9.	$S_4 \xrightarrow{h\nu} 2S_2$	Photochemical
10.	$S_4 \xrightarrow{h\nu} S_3 + S$	Photochemical
11.	$S + S_8 \rightarrow S_4 + S_5$	Two-body
12.	$S + S_7 \rightarrow 2S_4$	Two-body
13.	$S_2 + S_2 + M \rightarrow S_4 + M$	Three-body

S_4 are shown in Figures 8 and 9 for the M0 versus M1 and M1 versus M2 comparisons, respectively, in the Appendix.

Overall, imposing a 1 ppm lower-boundary sulfur mixing ratio produces enhancements of one to two orders of magnitude in the modeled S_3 and S_4 abundances, bringing them substantially closer to the observational constraints. This strong sensitivity indicates that the observed polysulfur chemistry on Venus cannot be reproduced without either an additional source of reduced sulfur from the deep atmosphere or surface, or more efficient formation pathways for S_3 and S_4 than those currently included in the XODIAC-2025.v1 and XODIAC-2025.v2 networks. Notably, the updates introduced from XODIAC-2025.v1 to XODIAC-2025.v2 do not significantly alter the resulting S_3 and S_4 mixing-ratio profiles. In other words, the missing sulfur problem likely reflects an unmodeled deep-atmosphere sulfur flux, missing reaction channels in the chemical network, or an underestimation of the efficiencies of the known polysulfur-forming pathways.

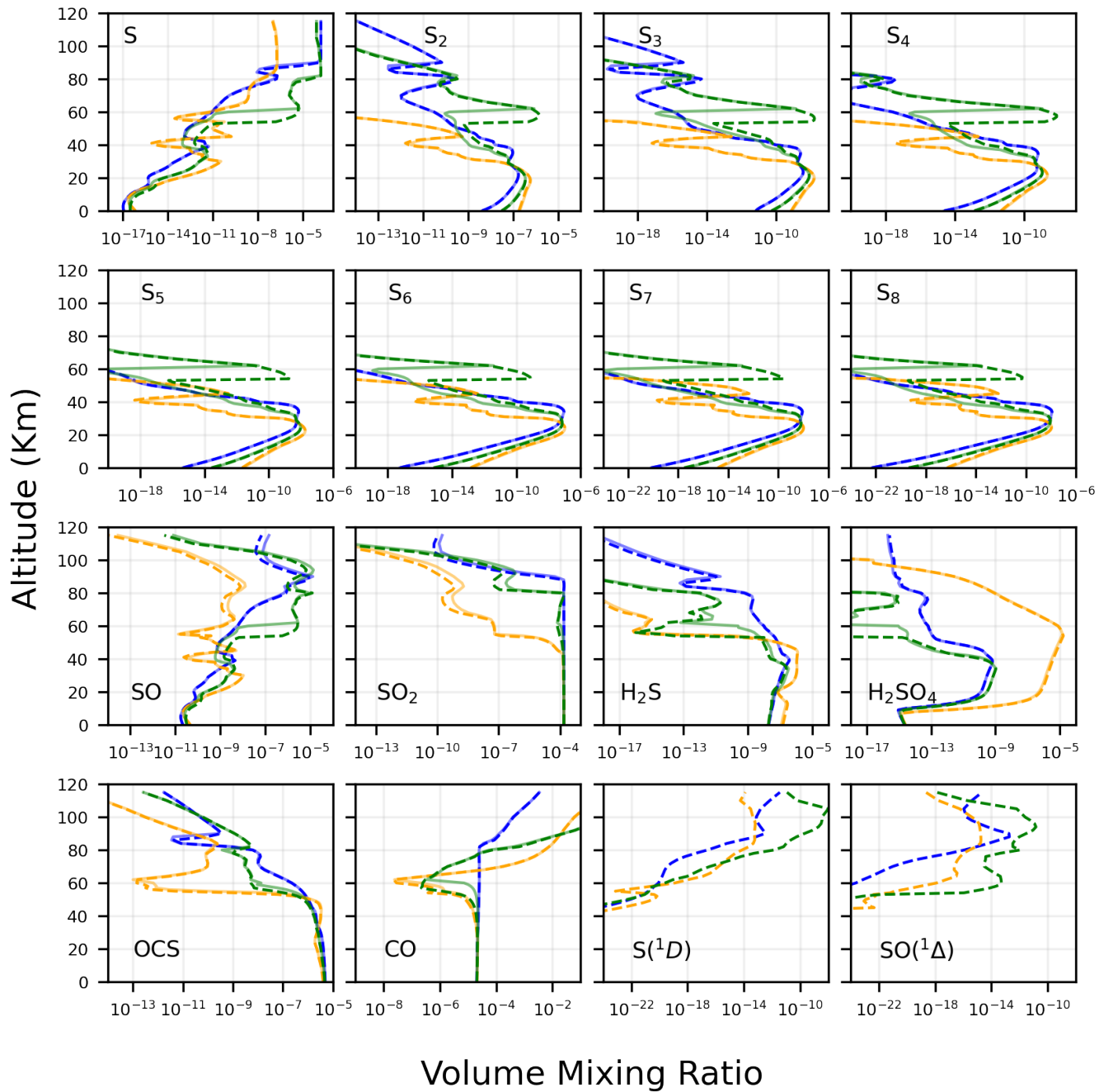


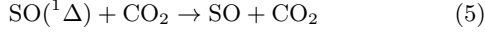
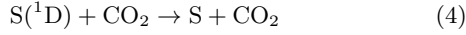
Figure 6. Predicted volume mixing ratios of S_n ($n = 1-8$), SO, SO_2 , H_2S , H_2SO_4 (gas + condensed), OCS, and CO as a function of altitude (km) in the exo-Venus atmosphere, using three models: M3 (blue; exo-Venus atmospheric profile from [Krasnopolsky \(2007\)](#) with a 505.6 K isotherm), M4 (orange; $1000\times$ solar flux at the top of the atmosphere), and M5 (green; combination of M3 and M4). Solid lines represent results from the XODIAC-2025.v1 network, and dashed lines represent those obtained with the XODIAC-2025.v2 network.

4.2.4. *Does the Extended XODIAC Chemical Network XODIAC-2025.v2, Including Excited $S(^1D)$ and $SO(^1\Delta)$, Produce Observable Differences in Sulfur Chemistry for Exo-Venus Analogs?*

Our Model M4 represents an exo-Venus analog characterized by an isothermal stratosphere above 30 km. In this scenario, only negligible changes are seen up to approximately 80 km, with minor variations appearing above this altitude (see Figure 6). This behavior arises because, although the isothermal layer is warmer than that of Venus, the reactions listed in Table 2 remain largely inefficient under these temperature conditions. The modest variations above ~ 80 km in SO, SO₂, and H₂S are primarily driven by the photochemical production of $S(^1D)$ and $SO(^1\Delta)$ via:

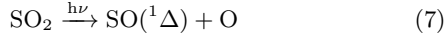


These excited species subsequently relax to their ground states through:



These reaction pathways and their corresponding rates are illustrated in Figure 10 (Appendix).

Our Model M5, which represents an exo-Venus analog subjected to $1000\times$ solar radiation, shows noticeable changes in the mixing ratios of sulfur species such as SO, SO₂, OCS, and CO above approximately 50 km. More pronounced variations in SO and SO₂ appear above ~ 60 km (see Figure 6). The enhanced stellar flux activates the photochemical pathways of SO₂, leading to its destruction through:



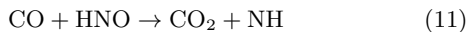
while SO is consumed through:



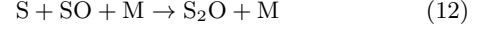
Because of the photochemical branch in reaction 7, the production of $SO(^1\Delta)$ in M5 is enhanced, which reduces the relative contribution of the ground-state channel in reaction 6 when compared to the XODIAC-2025.v1 network. In contrast, the base XODIAC-2025.v1 network produces SO additionally through:



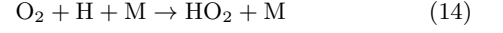
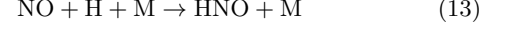
Finally, CO decreases in M5 around ~ 50 – 60 km as M5 has a comparatively faster rate of CO destruction (Figure 11) via:



The additional production of S₂O in XODIAC-2025.v1 is triggered due to SO (as the channel 7 is absent) through:

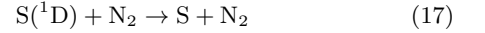
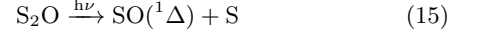


and HO₂ and HNO are produced from:



These reaction pathways are illustrated in Figure 11.

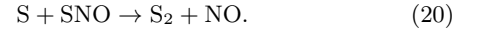
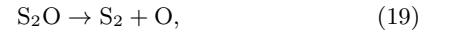
Among all simulations, Model M6 shows the largest changes in the mixing ratios of all species above approximately 30 km, as shown in Figure 6. These variations arise primarily from modifications to the dominant formation and destruction pathways caused by the additional reactions listed in Table 2 that are incorporated into the XODIAC-2025.v2 network. Figures 12 and 13 in the Appendix illustrate the key production and loss pathways for S, S₂, SO, SO₂, H₂S, and CO in the modeled exo-Venus analog atmospheres. In this network, the primary sulfur-bearing species are S and SO in both their ground and excited electronic states. Above ~ 30 km, the principal S production channels are:



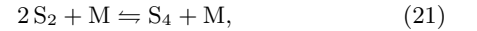
The enhanced production of atomic sulfur modifies the reaction rates of all S-bearing processes and reshapes the vertical distribution of S, which in turn regulates the polysulfur chemistry. For S₂, the key formation reactions are thermal decomposition of S₃:



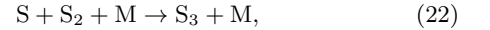
and reactions with other sulfur species:



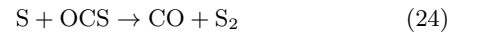
The key destruction reactions are also thermal decomposition:



and reactions with other sulfur allotropes:



The OCS molecule is also responsible for contributing to initializing the polysulfur chain of reactions through:



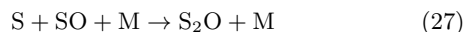
Around ~ 55 – 60 km, the rate of OCS destruction is dominated by reaction 24 in M6, which is higher by a few orders of magnitude compared to M0, where the dominating reaction is (Figure 12):



This reduction in rate of reaction 25 happens due to the equipartition of stellar energy across the channel 25 and its S(¹D) counterpart:



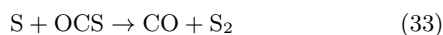
The major pathways forming S₂O and SNO in the region $\sim 35 - 60$ km are:



Once the polysulfur chain is initiated, a cascade of subsequent reactions propagates through higher-order allotropes, ultimately affecting species up to S₈. For other species such as SO and SO₂, their main sources of formation and loss are heterogenous chemistry exchanging sulfur to and from loud droplets, see [Rimmer et al. \(2021\)](#). The primary gas-phase drivers of abundance changes are reactions involving S and S₂O:

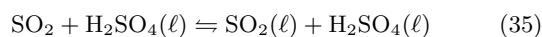


along with reactions 5 and 3. For CO, the dominant reactions effectively balance each other in exchange with OCS:



as well as reaction 11.

In Model M6, S(¹D) and SO(¹Δ) reach peak mixing ratios of order 10⁻⁸ and 10⁻¹¹, respectively, driven by the combined effects of the intense 1000× stellar irradiation and the 505.6 K isothermal profile. Photochemistry continuously produces these excited species, which subsequently relax to their ground states, thereby increasing the abundances of S and SO and enhancing their associated reaction pathways. Notably, unlike the Venusian models, reactions involving condensed SO₂ and H₂SO₄ are not dominant in M4 or M6 because the constant isotherm above ~ 30 km prevents efficient operation of:



These results highlight the importance of a high-altitude isotherm and intense stellar fluxes in controlling the sulfur photochemistry of exo-Venusian atmospheres. Altogether, our reaction network demonstrates that S-based reactions play a central role in shaping the chemical structure of exo-Venus atmospheres that experience elevated stellar radiation and/or sustained isothermal conditions above 30 km.

5. CONCLUSIONS

In this work, we introduced the extended XODIAC-2025 chemical network, XODIAC-2025.v2, for the fast, state-of-the-art 1D photochemical model XODIAC by incorporating excited-state sulfur chemistry and updated kinetic data suited to high-temperature, CO₂-dominated atmospheres. We applied this extended network to both Venus and exo-Venus analogs. Our key findings are summarized below:

1. The triplet S + CO₂ reaction proceeds through a two-step mechanism on the ground-state potential energy surface: an initiation step with a high entrance barrier of about 283 kJ/mol, followed by a low-barrier (<10 kJ/mol) dissociation to products.
2. Two pathways were identified on the singlet excited-state potential energy surface for the S + CO₂ reaction: one involving a single transition state and another involving the crossing of two high-energy transition states.
3. We constructed a comprehensive reaction network that includes thermochemical and photochemical processes involving S, SO, S(¹D), and SO(¹Δ) to quantify their impact on the abundances of sulfur-bearing molecules in Venusian and exo-Venusian atmospheres.
4. To update the thermochemical database for the newly added species in XODIAC-2025.v2, such as S(¹D) and SO(¹Δ), we computed their NASA polynomial coefficients, which had not been previously reported. These coefficients were validated against those of ground-state S and SO from the Burcat thermochemical database.
5. We validated the base XODIAC-2025.v1 network against the STAND-2020 network for Venus by incorporating condensation processes and the empirical parameterization of the unknown Venusian UV absorber.
6. Comparison of the XODIAC-2025.v1 and XODIAC-2025.v2 networks for Venus shows that the added reactions introduce negligible differences below 60 km, with only minor photochemically driven deviations at higher altitudes. Both networks reproduce the observed abundances of major sulfur-bearing species well, except for S₃ and S₄.
7. To assess the role of unaccounted sulfur sources on Venus, we compared two lower-boundary atomic sulfur conditions in XODIAC-2025.v2: zero sulfur and an imposed 1 ppm atomic sulfur abundance. Introducing 1 ppm S causes substantial increases in polysulfur abundances, particularly S₃ and S₄, bringing them into much closer agreement with observations. This result suggests the need for either a deeper, unmodeled source of reduced sulfur or more efficient polysulfur formation pathways than those presently included in existing networks.
8. We modeled three exo-Venus analogs: (i) a Venus-like P-T structure with an isotherm above 30 km, (ii) an atmosphere exposed to 1000× solar flux, and (iii) a hybrid of both. In all cases, sulfur chemistry is most

strongly modified above 30 km due to enhanced photochemical production of S and SO, which drives subsequent reaction cascades.

9. Our exo-Venus models (M4–M6) show increasing differences in sulfur abundances relative to the base XODIAC-2025.v1 network, driven primarily by the additional photochemical pathways introduced in XODIAC-2025.v2. Model M6 shows the largest deviations, followed by M5 and then M4, reflecting the combined influence of strong irradiation and the high-altitude isotherm.

ACKNOWLEDGMENTS

L.M. also extends thanks to Sukrit Ranjan of the Lunar and Planetary Laboratory, Department of Planetary Sci-

ences, University of Arizona, Tucson, USA, for insightful discussions on sulfur chemistry. L.M. acknowledges funding support from the DAE through the NISER project RNI 4011. L.M. also gratefully acknowledges support from Breakthrough Listen at the University of Oxford through a sub-award at NISER under Agreement R82799/CN013, provided as part of a global collaboration under the Breakthrough Listen project funded by the Breakthrough Prize Foundation. Part of this research was conducted at the Jet Propulsion Laboratory, California Institute of Technology under contract with the National Aeronautics and Space Administration (80NM0018D004). Support for K.W. was provided by NASA/Solar Systems Workings Program (19-SSW19-0291). N.R. thanks FONDECYT POSTDOCTOR-ADO (ANID, Chile) grant 3230221 for financial support.

APPENDIX

In this section, the profiles of the major reaction rates are shown for all models (M0 to M6) relevant to Venusian and exo-Venusian atmospheric chemistry in Figures 7 to 13. For the Venusian models, Figure 7 presents SO, SO₂, and H₂S, as their abundances vary the most between M0 and M2 (with no polysulfur variations). Figures 8 and 9 show the effects of adding 1 ppm atomic S and the associated polysulfur reactions involving S₂, S₃, and S₄, while keeping each network internally consistent.

For the exo-Venus models, Figure 10 illustrates the variations in S, SO, and SO₂ caused by the imposed stratospheric isotherm. Figure 11 shows how SO, SO₂, and CO respond to enhanced stellar radiation. Figures 12 and 13 present the reactions involving S, S₂, CO, SO, SO₂, and H₂S, as model M6 deviates the most from all other models.

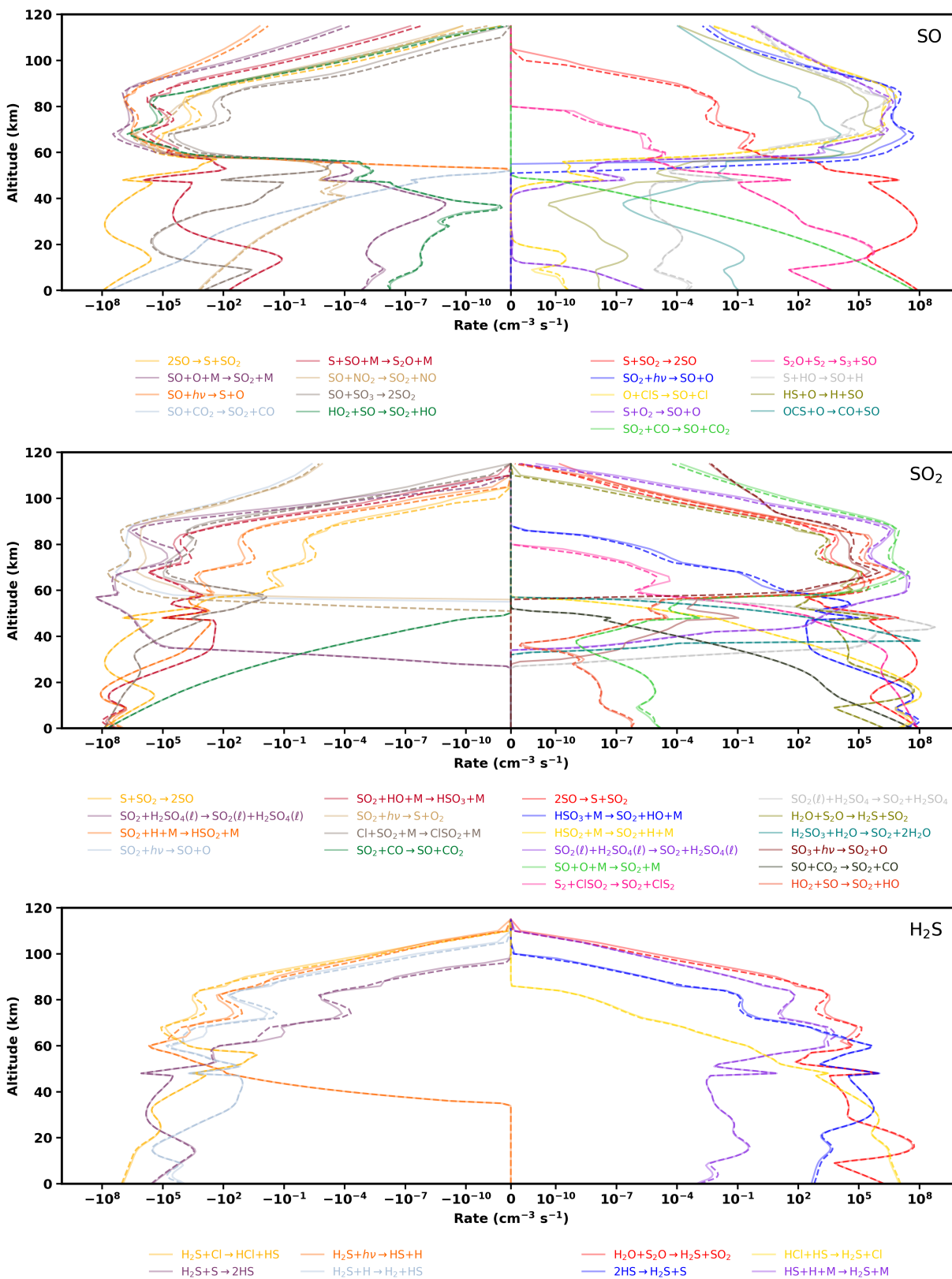


Figure 7. Rates of the major reactions with altitude in the Venus atmosphere for SO, SO₂, and H₂S. Solid and dashed lines correspond to results from the base XODIAC-2025.v1 network and the newly developed XODIAC-2025.v2 network, respectively. Reactions whose labels appear in dotted style are not included in the XODIAC-2025.v1 network. Negative rate values indicate that the reaction acts as a sink for the species, whereas positive values indicate a source. Symmetrical values on opposite sides of the zero rate for any reaction imply equal rates of formation and destruction. Reactions contributing less than 10% are omitted for clarity.

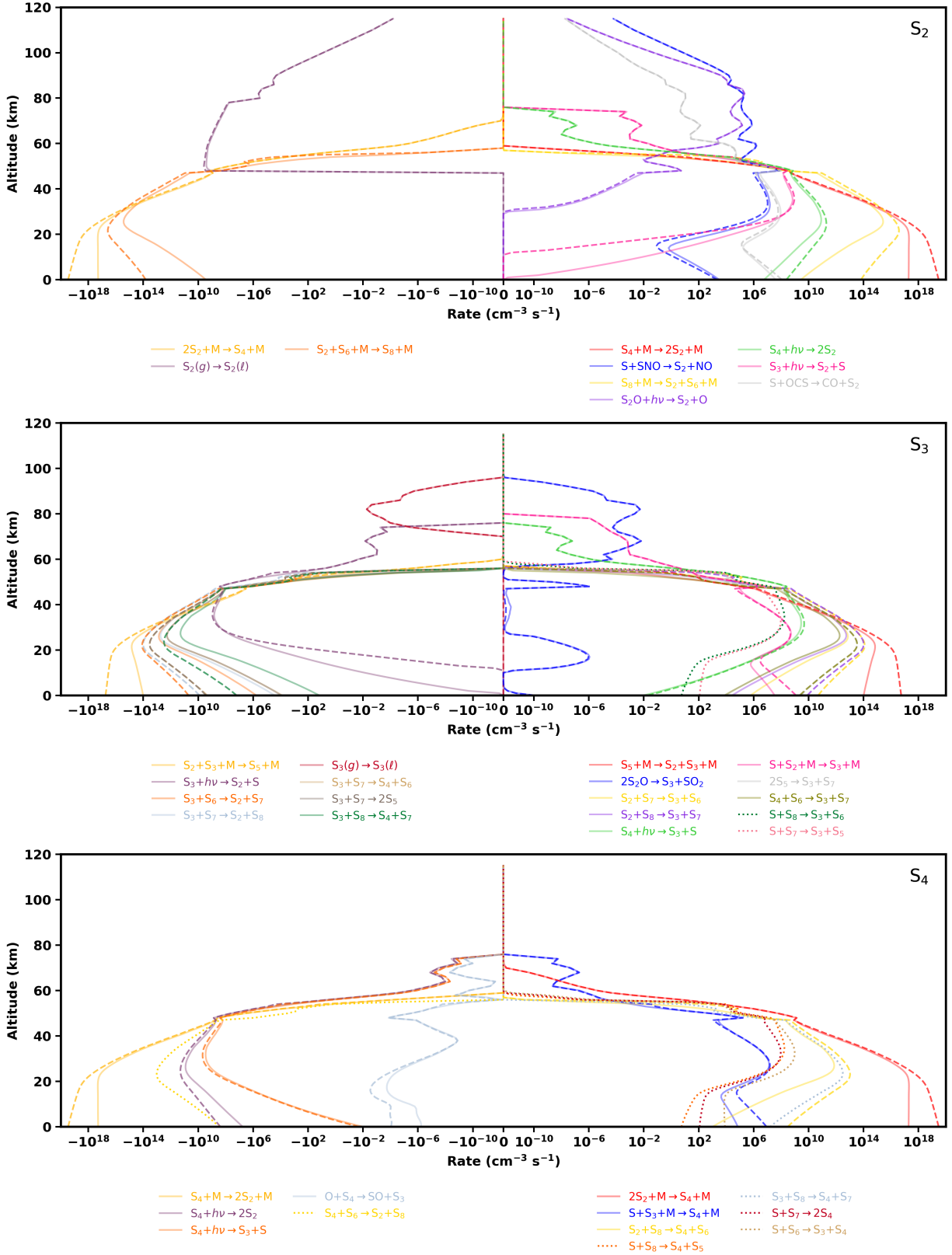


Figure 8. Rates of the major reactions with altitude in the Venus atmosphere for S₂, S₃ and S₄. Solid and dashed lines correspond to results from base XODIAC-2025.v1 network (M0) and XODIAC-2025.v1 with 1 ppm atomic S (M1), respectively. Reactions whose labels appear in dotted style are not included in the M0. Negative rate values indicate that the reaction acts as a sink for the species, whereas positive values indicate a source. Symmetrical values on opposite sides of the zero rate for any reaction imply equal rates of formation and destruction. Reactions contributing less than 10% are omitted for clarity.

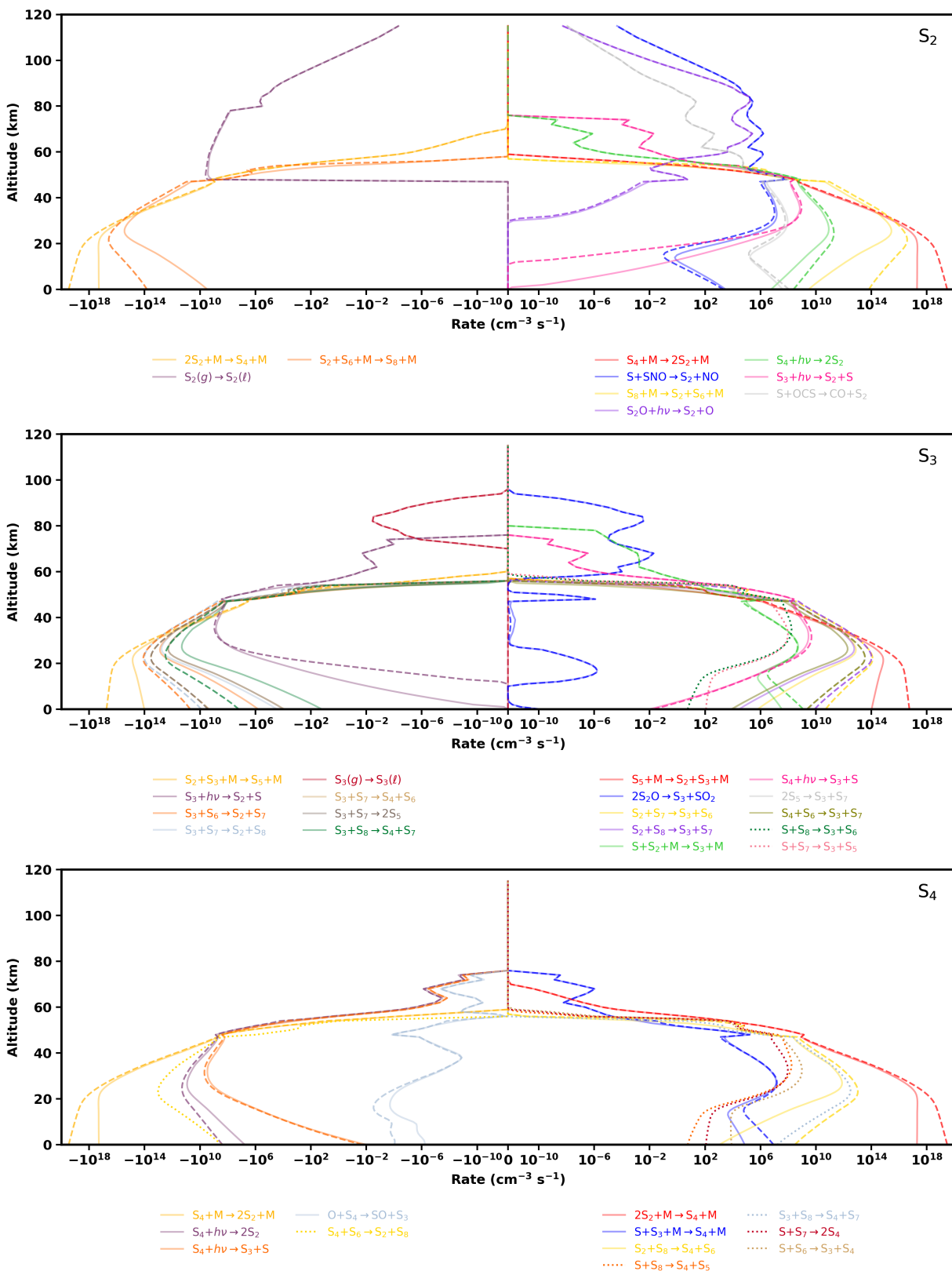


Figure 9. Rates of the major reactions with altitude in the Venus atmosphere for S_2 , S_3 and S_4 . Solid and dashed lines correspond to results from the newly developed XODIAC-2025.v2 network (M2) and XODIAC-2025.v2 with 1 ppm atomic S (M3), respectively. Reactions whose labels appear in dotted style are not included in M3. Negative rate values indicate that the reaction acts as a sink for the species, whereas positive values indicate a source. Symmetrical values on opposite sides of the zero rate for any reaction imply equal rates of formation and destruction. Reactions contributing less than 10% are omitted for clarity.

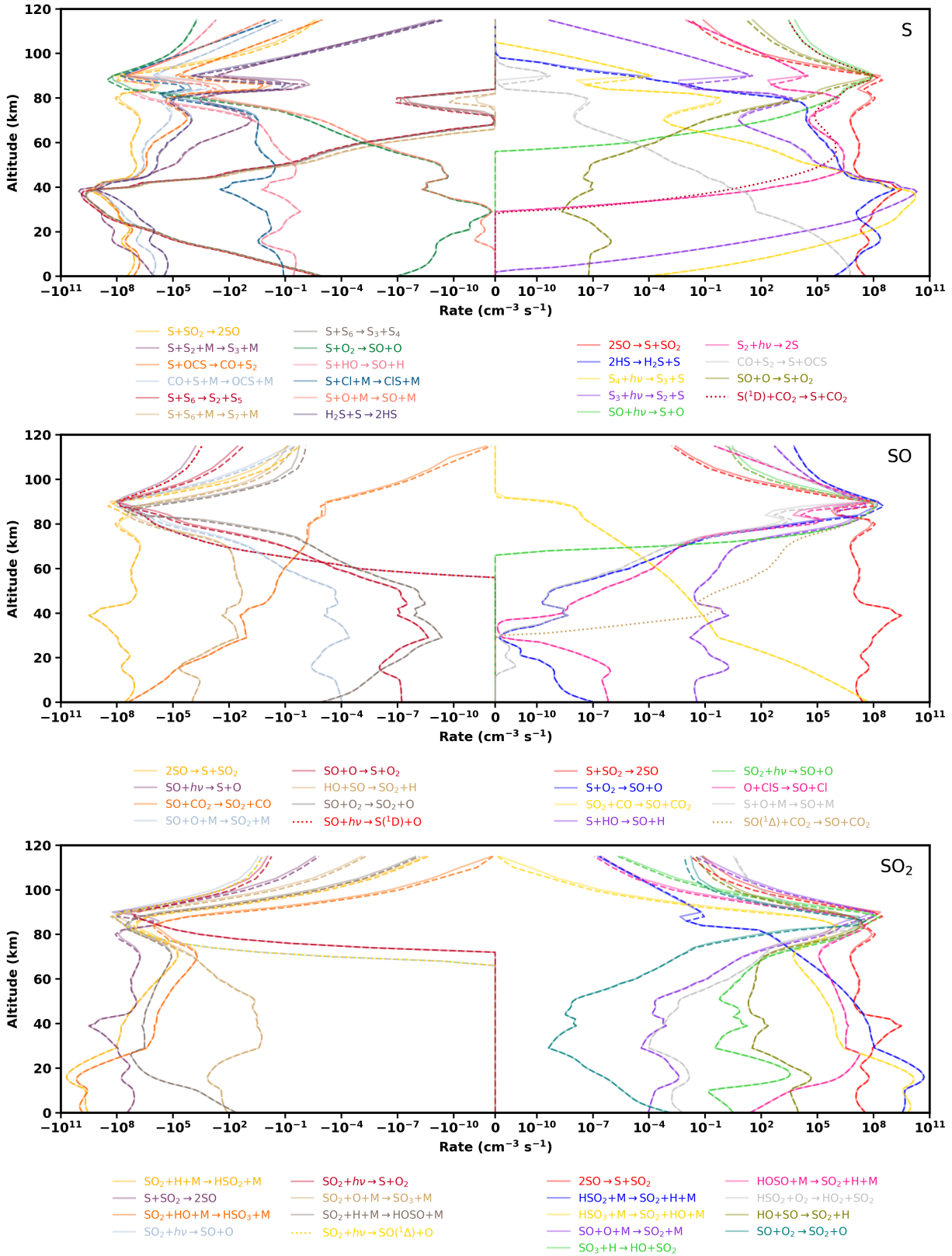


Figure 10. Rates of the major reactions as a function of altitude in the exo-Venus atmosphere (Model M4) for S, SO, and SO₂. Solid and dashed lines correspond to results from the base XODIAC-2025.v1 network and the newly developed XODIAC-2025.v2 network, respectively. Reactions whose labels appear in dotted style are not included in the XODIAC-2025.v1 network. Negative rate values indicate that the reaction acts as a sink for the species, whereas positive values indicate a source. Symmetrical values on opposite sides of the zero rate for any reaction imply equal rates of formation and destruction. Reactions contributing less than 10% are omitted for clarity.

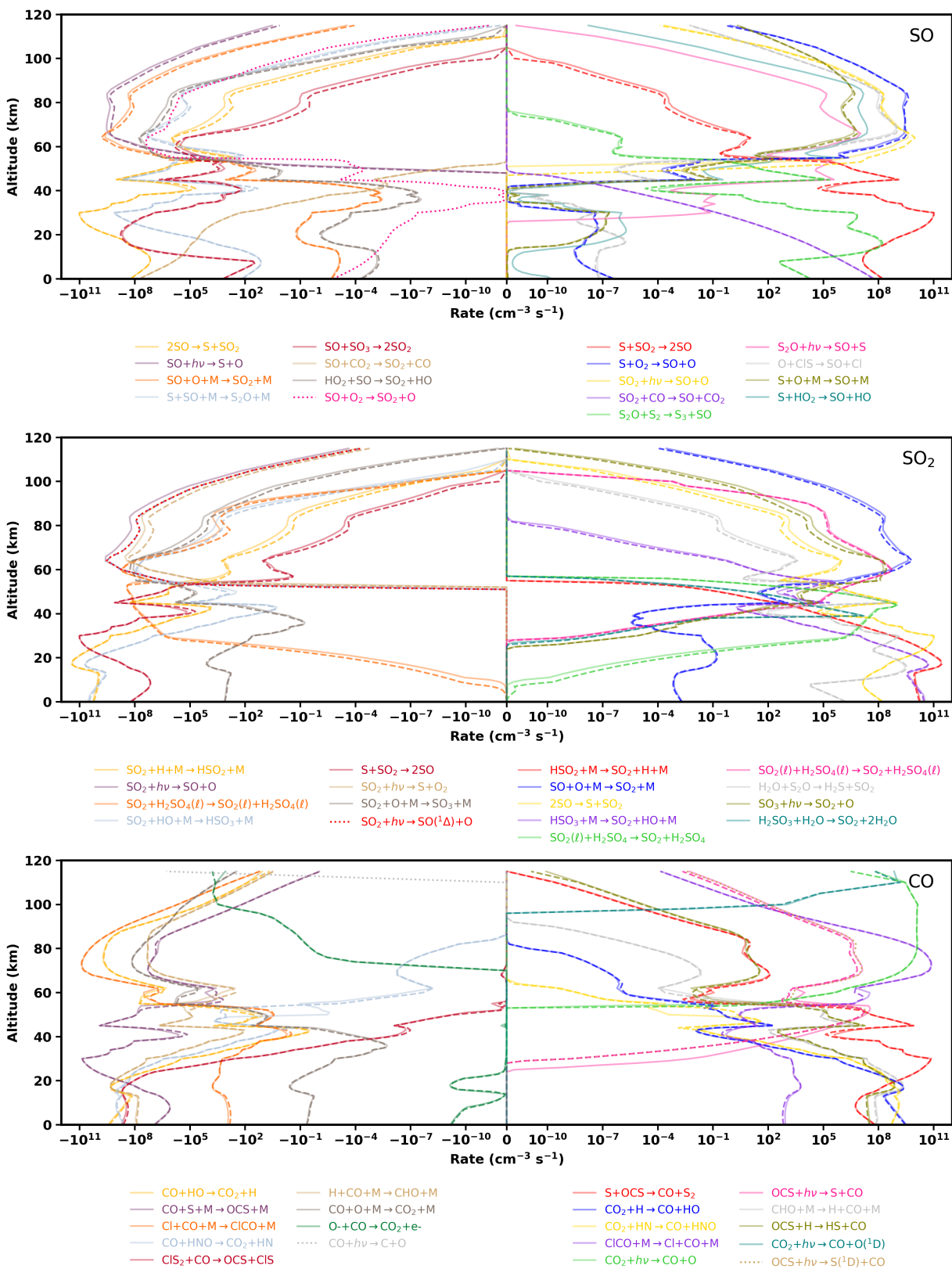


Figure 11. Same as Figure 10, but for the exo-Venus atmosphere (Model M5), showing the major reaction rates for SO, SO₂, and CO.

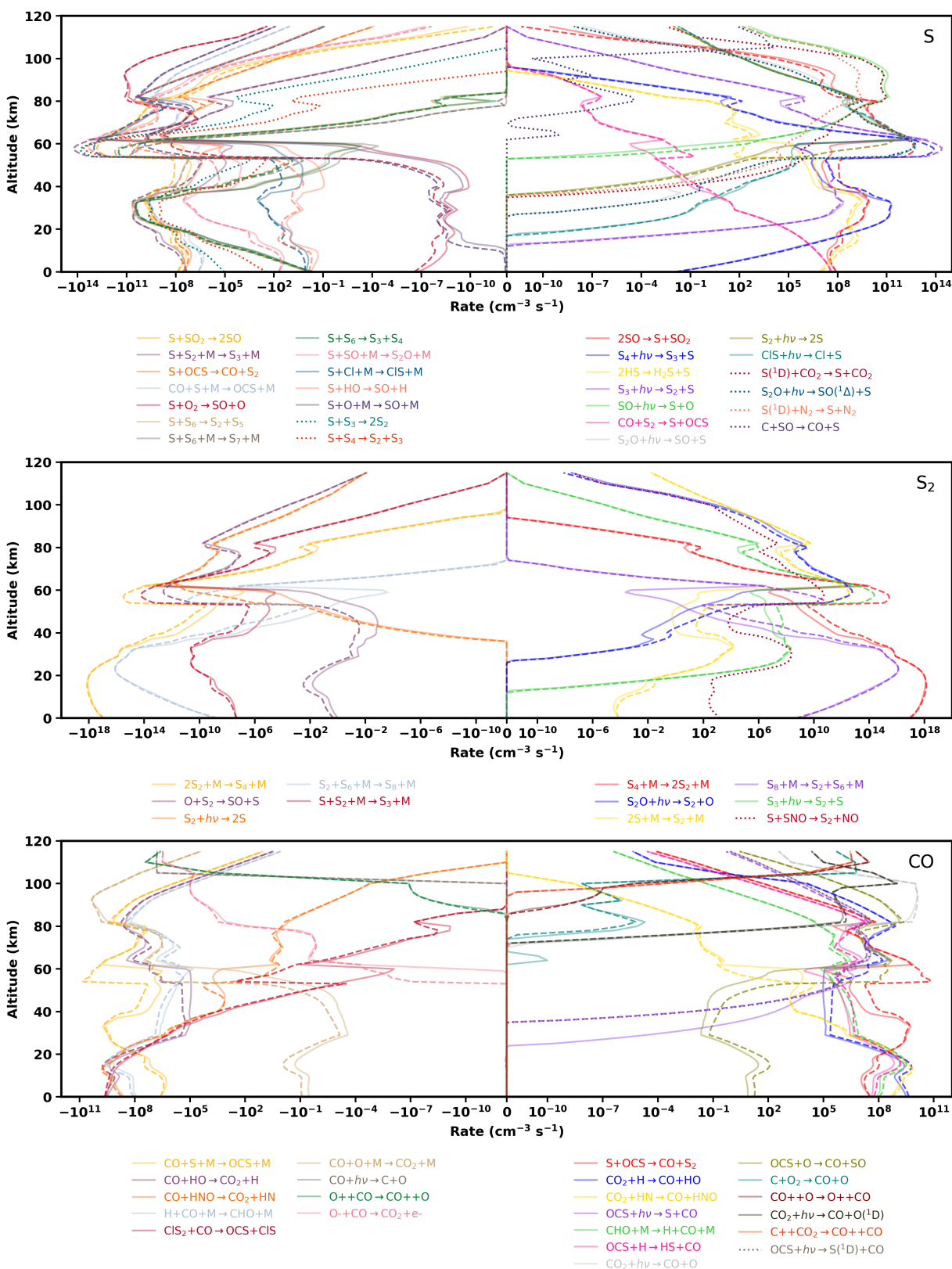


Figure 12. Same as Figure 10, but for the exo-Venus atmosphere (Model M6), showing the major reaction rates for S, S₂, and CO.

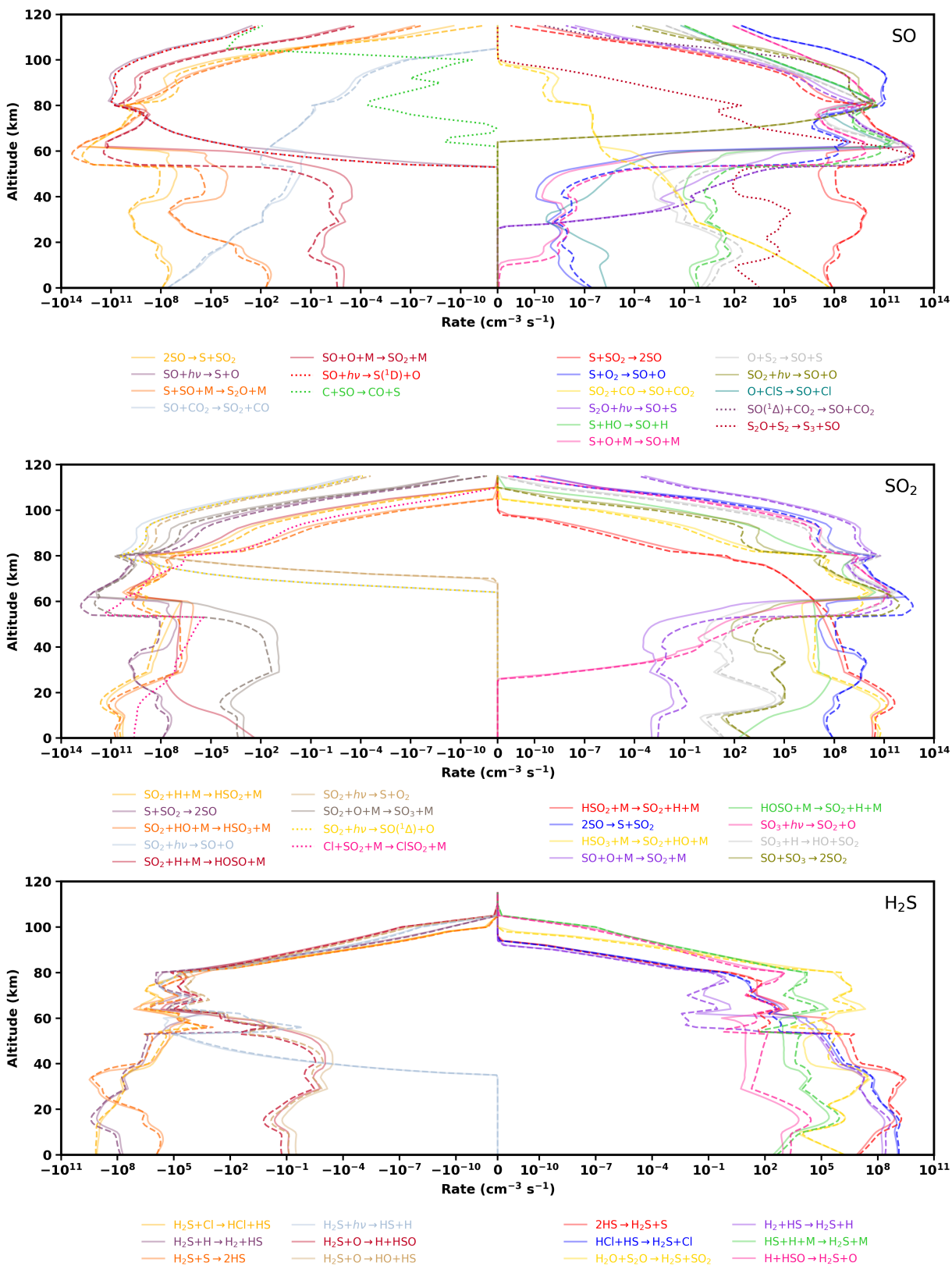


Figure 13. Same as Figure 10, but for the exo-Venus atmosphere (Model M6), showing the major reaction rates for SO, SO₂, and H₂S

REFERENCES

- Allen, M., Yung, Y. L., & Waters, J. W. 1981, *Journal of Geophysical Research: Space Physics*, 86, 3617, doi: <https://doi.org/10.1029/JA086iA05p03617>
- Arney, G., et al. 2014, *Journal of Geophysical Research: Planets*, 119, 1860, doi: [10.1002/2014JE004662](https://doi.org/10.1002/2014JE004662)
- Bao, J. L., & Truhlar, D. G. 2017, *Chemical Society Reviews*, 46, 7548
- Becke, A. 1993, *Density-Functional Thermochemistry. III. The Role of Exact Exchange*. *J. Chem. Phys.*, 98: 5648-5652
- Bello-Arufe, A., Damiano, M., Bennett, K. A., et al. 2025, *The Astrophysical Journal Letters*, 980, L26
- Bertaux, J. L., et al. 1996, *Journal of Geophysical Research*, 101, 12709, doi: [10.1029/96JE01083](https://doi.org/10.1029/96JE01083)
- Bézar, B., & de Bergh, C. 2007, *Journal of Geophysical Research: Planets*, 112, E04S07, doi: [10.1029/2006JE002794](https://doi.org/10.1029/2006JE002794)
- Bézar, B., et al. 1990, *Nature*, 345, 508, doi: [10.1038/345508a0](https://doi.org/10.1038/345508a0)
- Bierson, C. J., & Zhang, X. 2020, *Journal of Geophysical Research (Planets)*, 125, e06159, doi: [10.1029/2019JE006159](https://doi.org/10.1029/2019JE006159)
- Blečić, J., Harrington, J., & Bowman, M. O. 2016, *The Astrophysical Journal Supplement Series*, 225, 4, doi: [10.3847/0067-0049/225/1/4](https://doi.org/10.3847/0067-0049/225/1/4)
- Burcat, A., & Ruscic, B. 2005, *Third millenium ideal gas and condensed phase thermochemical database for combustion (with update from active thermochemical tables)*., Tech. rep., Argonne National Lab. (ANL), Argonne, IL (United States), doi: [10.2172/925269](https://doi.org/10.2172/925269)
- Burkholder, J. B., Sander, S. P., Abbatt, J. P. D., et al. 2019, *Chemical Kinetics and Photochemical Data for Use in Atmospheric Studies*, Evaluation No. 19, Tech. Rep. JPL Publication 19-5, Jet Propulsion Laboratory, California Institute of Technology, Pasadena, California. <http://jpldataeval.jpl.nasa.gov>
- Calmonte, U., Altwegg, K., Balsiger, H., et al. 2016, *Monthly Notices of the Royal Astronomical Society*, 462, S253, doi: [10.1093/mnras/stw2601](https://doi.org/10.1093/mnras/stw2601)
- Cavallotti, C., De Falco, C., Pratali Maffei, L., et al. 2020, *The journal of physical chemistry letters*, 11, 9621
- Coddington, O., Lean, J. L., Lindholm, D., et al. 2015, *NOAA Climate Data Record (CDR) of Solar Spectral Irradiance (SSI), NRLSSI Version 2*, NOAA National Centers for Environmental Information, doi: [10.7289/V51J97P6](https://doi.org/10.7289/V51J97P6)
- Collard, A. D., et al. 1993, *Planetary and Space Science*, 41, 487, doi: [10.1016/0032-0633\(93\)90032-9](https://doi.org/10.1016/0032-0633(93)90032-9)
- Connes, P., Connes, J., Kaplan, L. D., & Benedict, W. S. 1968, *The Astrophysical Journal*, 152, 731, doi: [10.1086/149590](https://doi.org/10.1086/149590)
- Cotton, D. V., et al. 2012, *Icarus*, 217, 570, doi: [10.1016/j.icarus.2011.05.020](https://doi.org/10.1016/j.icarus.2011.05.020)
- Dai, L., Shao, W., & Sheng, Z. 2024, *A&A*, 689, A55, doi: [10.1051/0004-6361/202450552](https://doi.org/10.1051/0004-6361/202450552)
- Dai, L., Titov, D. V., Shao, W. D., et al. 2025, *Space Science Reviews*, 221, 51, doi: [10.1007/s11214-025-01176-4](https://doi.org/10.1007/s11214-025-01176-4)
- Dana, A. G., Johnson, M. S., Allen, J. W., et al. 2023, *International Journal of Chemical Kinetics*, 55, 300, doi: <https://doi.org/10.1002/kin.21637>
- Deka, T., Khan, T. B., Dewan, S., et al. 2025, arXiv preprint arXiv:2504.18815. <https://arxiv.org/abs/2504.18815>
- DeWitt, H. L., Hasenkopf, C. A., Trainer, M. G., et al. 2010, *Astrobiology*, 10, 773
- Encrenaz, T., et al. 2012, *Astronomy & Astrophysics*, 543, A153, doi: [10.1051/0004-6361/201219419](https://doi.org/10.1051/0004-6361/201219419)
- . 2015, *Planetary and Space Science*, 113-114, 275, doi: [10.1016/j.pss.2015.01.011](https://doi.org/10.1016/j.pss.2015.01.011)
- Eva-Maria Ahrer, Lili Alderson, N. M. B. 2023, *Nature*, 614, 649
- Farquhar, J., Bao, H., & Thieme, M. 2000, *Science*, 289, 756
- Farquhar, J., Savarino, J., Airieau, S., & Thieme, M. H. 2001, *Journal of Geophysical Research: Planets*, 106, 32829
- Fegley, B. 2014, *Venus (Elsevier)*, 127-148, doi: [10.1016/B978-0-08-095975-7.01308-8](https://doi.org/10.1016/B978-0-08-095975-7.01308-8)
- Feinstein, A. D., Radica, M., Welbanks, L., et al. 2023, *Nature*, 614, 670
- Fernández-Ramos, A., Miller, J. A., Klippenstein, S. J., & Truhlar, D. G. 2006, *Chemical reviews*, 106, 4518
- Frisch, M. J., Trucks, G. W., Schlegel, H. B., et al. 2016, *Gaussian 16*, Revision A.03
- Fu, G., Welbanks, L., Deming, D., et al. 2024, *Nature*, 632, 752, doi: [10.1038/s41586-024-07760-y](https://doi.org/10.1038/s41586-024-07760-y)
- Fukui, K. 1981, *Accounts of chemical research*, 14, 363
- Gao, C. W., Allen, J. W., Green, W. H., & West, R. H. 2016, *Computer Physics Communications*, 203, 212
- Garvin, J. B., Getty, S. A., Arney, G. N., et al. 2022, *PSJ*, 3, 117, doi: [10.3847/PSJ/ac63c2](https://doi.org/10.3847/PSJ/ac63c2)
- Gelman, B. G., et al. 1979, *An Analysis of the Chemical Composition of the Atmosphere of Venus on an AMS of the Venera-12 Using a Gas Chromatograph*, Technical Memorandum NASA-TM-75476, NASA

- Georgievskii, Y., Miller, J. A., Burke, M. P., & Klippenstein, S. J. 2013, *The Journal of Physical Chemistry A*, 117, 12146
- Ghosh, P., Mishra, S., Dey, S., et al. 2025, arXiv e-prints, arXiv:2512.06729. <https://arxiv.org/abs/2512.06729>
- Grassi, D., et al. 2014, *Journal of Geophysical Research: Planets*, 119, 837, doi: [10.1002/2013JE004586](https://doi.org/10.1002/2013JE004586)
- Greaves, J. S., et al. 2020, *Nature Astronomy*, 5, 655, doi: [10.1038/s41550-020-1174-4](https://doi.org/10.1038/s41550-020-1174-4)
- He, C., Hörst, S. M., Lewis, N. K., et al. 2018, *ACS Earth and Space Chemistry*, 3, 39
- . 2020, *Nature Astronomy*, 4, 986
- Herrick, R. R., & Hensley, S. 2023, *Science*, 379, 1205, doi: [10.1126/science.abm7735](https://doi.org/10.1126/science.abm7735)
- Hobbs, R., Rimmer, P. B., Shorttle, O., & Madhusudhan, N. 2021, *Monthly Notices of the Royal Astronomical Society*, 506, 3186
- Hodgskiss, M. S. W., Crockford, P. W., Peng, Y., Wing, B. A., & Horner, T. J. 2019, *Proceedings of the National Academy of Sciences*, 116, 17207, doi: [10.1073/pnas.1900325116](https://doi.org/10.1073/pnas.1900325116)
- Hoffman, J. H., et al. 1980, *Journal of Geophysical Research*, 85, 7882, doi: [10.1029/JA085iA13p07882](https://doi.org/10.1029/JA085iA13p07882)
- Hörst, S. M., He, C., Lewis, N. K., et al. 2018, *Nature Astronomy*, 2, 303
- Hu, R., Bello-Arufe, A., Tokadjian, A., et al. 2025, arXiv preprint arXiv:2507.12622
- Huebner, W., & Mukherjee, J. 2015, *Planetary and Space Science*, 106, 11
- Huebner, W. F., & Carpenter, C. W. 1979, Solar photo rate coefficients
- Huebner, W. F., Keady, J. J., & Lyon, S. P. 1992, *Ap&SS*, 195, 1, doi: [10.1007/BF00644558](https://doi.org/10.1007/BF00644558)
- Irwin, P. G. 1999, *Surveys in geophysics*, 20, 505
- Jiang, C. Z., Rimmer, P. B., Lozano, G. G., et al. 2024, *Science Advances*, 10, eadg8826, doi: [10.1126/sciadv.adg8826](https://doi.org/10.1126/sciadv.adg8826)
- Johnson, M. S., Dong, X., Grinberg Dana, A., et al. 2022, *Journal of Chemical Information and Modeling*, 62, 4906, doi: [10.1021/acs.jcim.2c00965](https://doi.org/10.1021/acs.jcim.2c00965)
- Kama, M., Shorttle, O., Jermyn, A. S., et al. 2019, *The Astrophysical Journal*, 885, 114
- Kane, S. R., Arney, G., Crisp, D., et al. 2019, *Journal of Geophysical Research (Planets)*, 124, 2015, doi: [10.1029/2019JE005939](https://doi.org/10.1029/2019JE005939)
- Krasnopolsky, V. A. 2007, *Icarus*, 191, 25, doi: <https://doi.org/10.1016/j.icarus.2007.04.028>
- . 2008, *Icarus*, 197, 377, doi: [10.1016/j.icarus.2008.05.020](https://doi.org/10.1016/j.icarus.2008.05.020)
- . 2010, *Icarus*, 209, 314, doi: [10.1016/j.icarus.2010.05.008](https://doi.org/10.1016/j.icarus.2010.05.008)
- . 2012, *Icarus*, 218, 230, doi: <https://doi.org/10.1016/j.icarus.2011.11.012>
- . 2013, *Icarus*, 225, 570, doi: [10.1016/j.icarus.2013.04.026](https://doi.org/10.1016/j.icarus.2013.04.026)
- . 2014, *Icarus*, 237, 340, doi: [10.1016/j.icarus.2014.04.051](https://doi.org/10.1016/j.icarus.2014.04.051)
- Krishnan, R., Binkley, J. S., Seeger, R., & Pople, J. A. 1980, *The Journal of chemical physics*, 72, 650
- Laidler, K. J. 1996, *Pure and applied chemistry*, 68, 149
- Lee, C., Yang, W., & Parr, R. G. 1988, *Physical review B*, 37, 785
- Li, Y., Yu, Y., Zheng, Y., & Li, J. 2012, *Science China Chemistry*, 55, 1825
- Liggins, P. K. 2023, PhD thesis, University of Cambridge
- Liu, M., Grinberg Dana, A., Johnson, M. S., et al. 2021, *Journal of Chemical Information and Modeling*, 61, 2686, doi: [10.1021/acs.jcim.0c01480](https://doi.org/10.1021/acs.jcim.0c01480)
- Lodders, K. 2021, *Space Science Reviews*, 217, 44
- Macdonald, F. A., & Wordsworth, R. 2017, *Geophysical Research Letters*, 44, 1938, doi: <https://doi.org/10.1002/2016GL072335>
- Maiorov, B., et al. 2005, *Solar System Research*, 39, 267, doi: [10.1007/s11208-005-0039-9](https://doi.org/10.1007/s11208-005-0039-9)
- Malin, G. 1997, *Nature*, 387, 857
- Marcq, E., et al. 2005, *Icarus*, 179, 375, doi: [10.1016/j.icarus.2005.06.018](https://doi.org/10.1016/j.icarus.2005.06.018)
- . 2006, *Planetary and Space Science*, 54, 1360, doi: [10.1016/j.pss.2006.04.024](https://doi.org/10.1016/j.pss.2006.04.024)
- . 2008, *Journal of Geophysical Research*, 113, E00B07, doi: [10.1029/2008JE003074](https://doi.org/10.1029/2008JE003074)
- . 2015, *Planetary and Space Science*, 113-114, 256, doi: [10.1016/j.pss.2015.02.011](https://doi.org/10.1016/j.pss.2015.02.011)
- Matthes, K., Funke, B., Andersson, M. E., et al. 2017, *Geoscientific Model Development*, 10, 2247, doi: [10.5194/gmd-10-2247-2017](https://doi.org/10.5194/gmd-10-2247-2017)
- Miller, J. A., & Klippenstein, S. J. 2006, *The Journal of Physical Chemistry A*, 110, 10528
- Mollière, P., van Boekel, R., Bouwman, J., et al. 2017, *A&A*, 600, A10, doi: [10.1051/0004-6361/201629800](https://doi.org/10.1051/0004-6361/201629800)
- Moses, J. I., Allen, M., & Gladstone, G. R. 1995, *Geophysical research letters*, 22, 1597
- Moses, J. I., Zolotov, M. Y., & Fegley Jr, B. 2002, *Icarus*, 156, 76
- Moses, J. I., Visscher, C., Fortney, J. J., et al. 2011, *The Astrophysical Journal*, 737, 15
- Moses, J. I., Marley, M. S., Zahnle, K., et al. 2016, *The Astrophysical Journal*, 829, 66
- Mukhin, L. M., et al. 1982, *Soviet Astronomy Letters*, 8, 216
- . 1983, *Venera-13, Venera-14: Chemical analysis of Venus atmosphere*

- Na, C. Y., et al. 1990, *Journal of Geophysical Research*, 95, 7485, doi: [10.1029/JD095iD06p07485](https://doi.org/10.1029/JD095iD06p07485)
- Ono, S., Eigenbrode, J. L., Pavlov, A. A., et al. 2003, *Earth and Planetary Science Letters*, 213, 15
- Oschlisniok, A., et al. 2012, *Icarus*, 221, 940, doi: [10.1016/j.icarus.2012.09.020](https://doi.org/10.1016/j.icarus.2012.09.020)
- Oyama, V. I., et al. 1979, *Science*, 203, 802, doi: [10.1126/science.203.4382.802](https://doi.org/10.1126/science.203.4382.802)
- . 1980, *Journal of Geophysical Research*, 85, 7891, doi: [10.1029/JA085iA13p07891](https://doi.org/10.1029/JA085iA13p07891)
- Pavlov, A., & Kasting, J. 2002, *Astrobiology*, 2, 27
- Petralia, A., Alei, E., Aresu, G., et al. 2020, *Monthly Notices of the Royal Astronomical Society*, 496, 5350
- Pollack, J. B., et al. 1993, *Icarus*, 103, 1, doi: [10.1006/icar.1993.1055](https://doi.org/10.1006/icar.1993.1055)
- Raghavachari, K., Trucks, G. W., Pople, J. A., & Head-Gordon, M. 1989, *Chemical Physics Letters*, 157, 479
- Ranjan, S., Schwieterman, E. W., Harman, C., et al. 2020, *ApJ*, 896, 148, doi: [10.3847/1538-4357/ab9363](https://doi.org/10.3847/1538-4357/ab9363)
- Recio, P., Alessandrini, S., Vanuzzo, G., et al. 2022, *Nature Chemistry*, 14, 1405
- Reed, N. W., Browne, E. C., & Tolbert, M. A. 2020, *ACS Earth and Space Chemistry*, 4, 897
- Reed, N. W., Shearer, R. L., McGlynn, S. E., et al. 2024, *The Astrophysical Journal Letters*, 973, L38
- Reed, N. W., Wing, B. A., Tolbert, M. A., & Browne, E. C. 2022, *Geophysical Research Letters*, 49, e2021GL097032
- Rimmer, P. B., & Helling, C. 2016, *ApJS*, 224, 9, doi: [10.3847/0067-0049/224/1/9](https://doi.org/10.3847/0067-0049/224/1/9)
- Rimmer, P. B., Jordan, S., Constantinou, T., et al. 2021, *PSJ*, 2, 133, doi: [10.3847/PSJ/ac0156](https://doi.org/10.3847/PSJ/ac0156)
- Spencer, J. R., Jessup, K. L., McGrath, M. A., Ballester, G. E., & Yelle, R. 2000, *Science*, 288, 1208
- Stock, J. W., Kitzmann, D., Patzer, A. B. C., & Sedlmayr, E. 2018, *Monthly Notices of the Royal Astronomical Society*, 479, 865, doi: [10.1093/mnras/sty1531](https://doi.org/10.1093/mnras/sty1531)
- Swain, M. R., Estrela, R., Roudier, G. M., et al. 2021, *The Astronomical Journal*, 161, 213
- Titov, D. V., Ignatiev, N. I., McGouldrick, K., Wilquet, V., & Wilson, C. F. 2018, *Space Science Reviews*, 214, 1
- Tsai, S.-M., Lyons, J. R., Grosheintz, L., et al. 2017, *The Astrophysical Journal Supplement Series*, 228, 20, doi: [10.3847/1538-4365/228/2/20](https://doi.org/10.3847/1538-4365/228/2/20)
- Tsai, S.-M., Malik, M., Kitzmann, D., et al. 2021, *The Astrophysical Journal*, 923, 264
- Tsai, S.-M., Lee, E. K., Powell, D., et al. 2023, *Nature*, 617, 483
- Tsang, C. C. C., et al. 2008, *Journal of Geophysical Research*, 113, E00B08, doi: [10.1029/2008JE003089](https://doi.org/10.1029/2008JE003089)
- Turrini, D., Schisano, E., Fonte, S., et al. 2021, *The Astrophysical Journal*, 909, 40, doi: [10.3847/1538-4357/abd6e5](https://doi.org/10.3847/1538-4357/abd6e5)
- Veillet, R., Venot, O., Sirjean, B., et al. 2024, *Astronomy & Astrophysics*, 682, A52
- . 2025, arXiv preprint arXiv:2505.12152, doi: [10.48550/arXiv.2505.12152](https://doi.org/10.48550/arXiv.2505.12152)
- Venot, O., Hébrard, E., Agúndez, M., et al. 2012, *A&A*, 546, A43, doi: [10.1051/0004-6361/201219310](https://doi.org/10.1051/0004-6361/201219310)
- Wakelam, V., Herbst, E., Loison, J. C., et al. 2012, *ApJS*, 199, 21, doi: [10.1088/0067-0049/199/1/21](https://doi.org/10.1088/0067-0049/199/1/21)
- Willacy, K., Chen, S., Adams, D. J., & Yung, Y. L. 2022, *The Astrophysical Journal*, 933, 230
- Wilson, C. F., et al. 1981, *Icarus*, 45, 624, doi: [10.1016/0019-1035\(81\)90023-2](https://doi.org/10.1016/0019-1035(81)90023-2)
- Wogan, N. F., Batalha, N. E., Zahnle, K., et al. 2025, *PSJ*, 6, 256, doi: [10.3847/PSJ/ae0e1c](https://doi.org/10.3847/PSJ/ae0e1c)
- Woitke, P., Herbort, O., Helling, C., et al. 2021, *Astronomy & Astrophysics*, 646, A43
- Woitke, P., Helling, Ch., Hunter, G. H., et al. 2017, *A&A*, 614, A1, doi: [10.1051/0004-6361/201732193](https://doi.org/10.1051/0004-6361/201732193)
- Yang, J., Gudipati, M. S., Henderson, B. L., & Fleury, B. 2023, *The Astrophysical Journal*, 947, 26, doi: [10.3847/1538-4357/acbd9b](https://doi.org/10.3847/1538-4357/acbd9b)
- Yang, J., & Hu, R. 2024a, *The Astrophysical Journal Letters*, 971, L48
- . 2024b, *The Astrophysical Journal*, 966, 189, doi: [10.3847/1538-4357/ad35c8](https://doi.org/10.3847/1538-4357/ad35c8)
- Young, L. D. G. 1972, *Icarus*, 17, 632, doi: [10.1016/0019-1035\(72\)90029-2](https://doi.org/10.1016/0019-1035(72)90029-2)
- Zahnle, K., Mac Low, M.-M., Lodders, K., & Fegley Jr., B. 1995, *Geophysical Research Letters*, 22, 1593, doi: [https://doi.org/10.1029/95GL01190](https://doi.org/https://doi.org/10.1029/95GL01190)
- Zahnle, K., Marley, M. S., Morley, C. V., & Moses, J. I. 2016, *The Astrophysical Journal*, 824, 137
- Zasova, L. V., et al. 1993, *Icarus*, 105, 92, doi: [10.1006/icar.1993.1113](https://doi.org/10.1006/icar.1993.1113)
- Zhang, X., Liang, M. C., Mills, F. P., Belyaev, D. A., & Yung, Y. L. 2012, *Icarus*, 217, 714
- Zhao, Y., & Truhlar, D. G. 2008, *Theoretical chemistry accounts*, 120, 215